Available online at www.sciencedirect.com
ScienceDirect
Bioorganic & Medicinal Chemistry 14 (2006) 6640–6658
Bioorganic & Medicinal Chemistry

# Novel ligands for the human histamine $H_1$ receptor: Synthesis, pharmacology, and comparative molecular field analysis studies of 2-dimethylamino-5-(6)-phenyl-1,2,3,4-tetrahydronaphthalenes

Ola M. Ghoneim,[a] Jacqueline A. Legere,[a] Alexander Golbraikh,[a] Alexander Tropsha[a] and Raymond G. Booth[b,*]

[a]*Division of Medicinal Chemistry and Natural Products, School of Pharmacy, University of North Carolina at Chapel Hill, Chapel Hill, NC 27599-7360, USA*
[b]*Department of Medicinal Chemistry, PO Box 100485, College of Pharmacy, University of Florida, Gainesville, FL 32610-0485, USA*

Received 10 April 2006; revised 31 May 2006; accepted 31 May 2006
Available online 16 June 2006

**Abstract**—This paper reports the synthesis of a novel series of (±)-2-dimethylamino- 5- and 6-phenyl-1,2,3,4-tetrahydronaphthalene derivatives (5- and 6-APTs), and, corresponding affinity, functional activity, and, molecular modeling studies with regard to drug design targeting the human histamine $H_1$ receptor. The 5-APTs have 2- to 4-fold higher $H_1$ receptor affinity than the endogenous agonist histamine. The chemical nature of a *meta*-substituent on the 5-APT pendant phenyl moiety does not significantly affect $H_1$ affinity. In contrast, analogous *meta*-substitution for the 6-APTs increases $H_1$ affinity up to 100-fold. The new APTs do not activate $H_1$ receptor-linked intracellular signaling and apparently are competitive $H_1$ antagonists. A new model that establishes structural parameters for binding to the human $H_1$ receptor by APTs and other ligands was developed using 3-D QSAR (CoMFA). The model predicts $H_1$ ligand binding with a higher degree of external predictability compared to a previously reported model. The APTs also were examined for activity at human serotonin 5-$HT_{2A}$ and 5-$HT_{2C}$ receptors, which are phylogenetically closely related to the $H_1$ receptor. 5-APT and *m*-Cl-6-APT were identified as novel agonists that selectively activate 5-$HT_{2C}$ receptors. It is concluded that the lipophilic (brain-penetrating) APT molecular scaffold may have pharmacotherapeutic potential in neuropsychiatric diseases.


## 1. Introduction

The biogenic amine histamine (2-[imidazol-4-yl]-ethylamine; **1**, Fig. 1) is a chemical messenger involved in diverse functions, including, neurotransmission, gastric acid secretion, and smooth muscle contraction.[1] The effects of histamine are mediated by four G protein-coupled receptors (GPCRs), classified as $H_1$, $H_2$, $H_3$, and $H_4$. The $H_1$ receptor was first cloned and characterized from bovine adrenal gland in 1991.[2] Soon after, the genes encoding the $H_1$ receptor from other species, including human, were cloned.[3] Southern blot analysis with $H_1$ receptor probes indicates that there are no related genes in various species and there is no compelling evidence for $H_1$ receptor subtypes,[4] though, inter-species heterogeneity regarding $H_1$ pharmacology is known.[5] As is the case for other GPCRs except rhodopsin, the three-dimensional structure of the $H_1$ receptor is unknown.

In mammalian smooth muscle, endothelial, and brain tissue, histamine activation of $H_1$ receptors predominately triggers $G\alpha_q$ protein activation with subsequent stimulation of phospholipase (PL) C and formation of inositol phosphates (IP) and diacylglycerol.[1] This activity can present clinically as respiratory distress (bronchial constriction), diarrhea (GI contractions), and edema and hypotension (increased vascular permeability), especially associated with the peripheral allergic response. In mammalian brain and adrenal gland, $H_1$ receptors can stimulate adenylyl cyclase (AC) and formation of adenosine 3′,5′-cyclic monophosphate (cAMP),[6,7] that can lead to activation of catecholamine neurotransmitter synthesis and release.[8–12]

*Keywords*: GPCR; Histamine receptor; Inositol phosphates; Intracellular signaling; Molecular modeling; Neurotransmitter; PLC; QSAR; Serotonin receptor; Tetrahydronaphthalene.
* Corresponding author. Tel.: +1 352 846 1953; fax: +1 352 392 9455; e-mail: Booth@cop.ufl.edu

0968-0896/$ - see front matter © 2006 Elsevier Ltd. All rights reserved.
doi:10.1016/j.bmc.2006.05.077

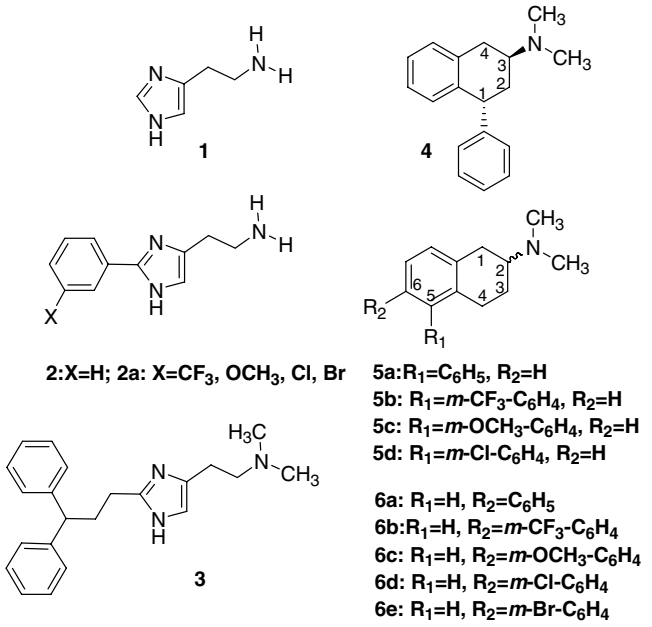


**Figure 1.** Structures of known (**1**–**3**) and proposed (**4**–**6**) $H_1$ ligands: histamine (**1**), 2-phenylhistamines (**2**), dimethylhistaprodifen (**3**), (−)-*trans*-PAT (**4**), 5-APTs (**5**), and 6-APTs (**6**).

Research and development of $H_1$ ligands largely has focused on antagonists[13] that are used for their anti-allergy effects in the periphery. Recent understanding of the clinical importance of $H_1$ receptors in brain, however, suggests the pharmacotherapeutic potential of $H_1$ agonists in neurodegenerative and neuropsychiatric disorders. For example, certain $H_1$ agonists can stimulate mammalian forebrain catecholamine neurotransmitter (dopamine, norepinephrine) synthesis in vitro[8,9] and in vivo.[10] In this regard, deficiency of forebrain dopamine neurotransmission accounts for the clinical manifestations of the neurodegenerative disorder Parkinson's disease. Also, dysfunction of brain catecholamine neurotransmission contributes to the cause and/or treatment of several neuropsychiatric disorders, including, depression, schizophrenia, manic-depressive illness, and drug addiction.[14–16] Other putative physiological functions of brain $H_1$ receptors include modulation of appetite, arousal, mood, and behavior.[1]

About 25 years ago, the first selective $H_1$ agonists, based on derivatives of histamine substituted at the imidazole ring position C2, were reported, for example, 2-phenylhistamine (**2**, Fig. 1).[17] Although **2** is selective for $H_1$ receptors, its affinity is not improved over histamine and it is a partial agonist.[5,18] Introduction of substituents at the *meta*-position of the phenyl ring of **2**, including electron-donating and -withdrawing groups (e.g., methoxy, trifluoromethyl, chloro, and bromo; **2a**, Fig. 1), can yield selective $H_1$ ligands with up to ~10 times improved affinity compared to histamine, though, agonist efficacy is only partial.[5,19–21] Replacement of the 2-phenyl moiety of **2** with a 3,3-diphenylpropyl moiety led to development of the histaprodifen-type $H_1$ agonists, with the $N^{\alpha}$,$N^{\alpha}$-dimethyl analog (dimethylhistaprodifen; **3**, Fig. 1) reported as having 5 times higher affinity than histamine, but, only partial agonist activity at the human $H_1$ receptor[5,22,23] and antagonist activity at the bovine $H_1$ receptor.[24] Development of $H_1$ agonists structurally divergent from the 2-phenylhistamine and histaprodifen types includes substituted analogs of 1-phenyl-3-dimethylamino-1,2,3,4-tetrahydronaphthalene (PAT), the most potent being (1*R*, 3*S*)-(−)-*trans*-PAT (**4**, Fig. 1).[9,25] The (−)-*trans*-PAT isomer has high $H_1$ affinity ($K_i \sim 1.0$ nM) and is an $H_1$ agonist that activates catecholamine neurotransmitter synthesis in mammalian forebrain in vitro and in vivo, with efficacy equivalent to histamine.[7,10]

In an effort to further probe the $H_1$ receptor binding and functional pharmacophores, we report here on a series of novel (±)-2-dimethylamino- 5- and 6-phenyl-1,2,3,4-tetrahydronaphthalenes (5- and 6-APTs, Fig. 1). The APTs represent a hybrid structure of the molecular scaffolds of 2-phenylhistamine (**2**)/histaprodifen (**3**) type, and, PAT type (**4**) $H_1$ agonists. Structural similarity of the APTs and PATs is obvious (Fig. 1) and the energy minimized structure of the APTs in comparison to **2** and **3** (Fig. 2) indicates several common steric and electronic features, including, the terminal amine moiety, aromatic ring scaffold, and appended phenyl moiety. This paper includes the synthesis of 5- and 6-APT and several *meta*-substituted analogs (**5b**–**d**, **6b**–**e**; Fig. 1), corresponding to **2a**, as well as, their affinity and functional activity at the cloned human histamine $H_1$ receptor (in comparison to phylogenetically related serotonin $5HT_2$ receptors). Also reported here is a three-dimensional quantitative structure–affinity relationship (3D QSAR) model for binding of APTs and other $H_1$ receptor ligands, which is a refinement of a previously reported model.[27]

## 2. Results

### 2.1. Chemistry

Scheme 1 shows the synthetic method to provide 5-APTs (**5a**–**d**). The 5-(*m*-substituted)-phenyl-1-tetralone intermediates (**12a**–**d**) were obtained via Suzuki–Miyaura palladium-catalyzed cross-coupling[28,29] of 5-bromo-1-tetralone (**11**) with the appropriate phenylboronic acid (PBA). The resulting 1-tetralones were transposed to 2-tetralones by reducing the 1-ketone to the alcohol, followed by dehydration to form the 1,2-alkene. Epoxidation of the alkene with *m*-chloroperoxybenzoic acid (*m*CPBA) and semipinacol rearrangement with boron trifluoride etherate[30] gave the corresponding 2-tetralones (**13a**–**d**). Reductive amination of the 2-tetralones gave the racemic 5-APTs (**5a**–**d**) for initial pharmacological testing.

Scheme 2 shows the synthesis of 6-APT (**6a**) from 4-biphenylacetic acid (**14**). The acid chloride (**15**) was formed and added dropwise to a slurry of aluminum chloride in $CH_2Cl_2$ under a stream of ethylene gas according to a modification[31] of the Burckhalter and Campbell[32] method. Ring closure was indicated by two triplets in the $^1H$ NMR spectrum, representing

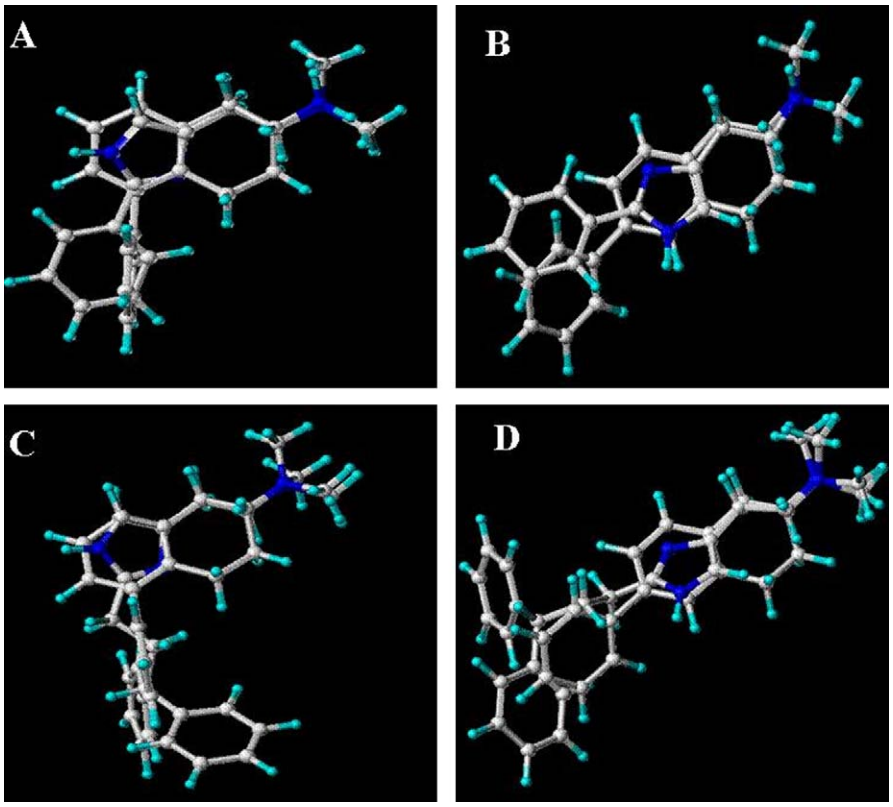


**Figure 2.** (A) Structural features shared by 5-APT and 2-phenylhistamine (RMS = 0.217 Å); (B) Structural features shared by 6-APT and 2-phenylhistamine (RMS = 0.298 Å); (C) Structural features shared by 5-APT and dimethylhistaprodifen (RMS = 0.152 Å); (D) Structural features shared by 6-APT and dimethylhistaprodifen (RMS = 0.305 Å).

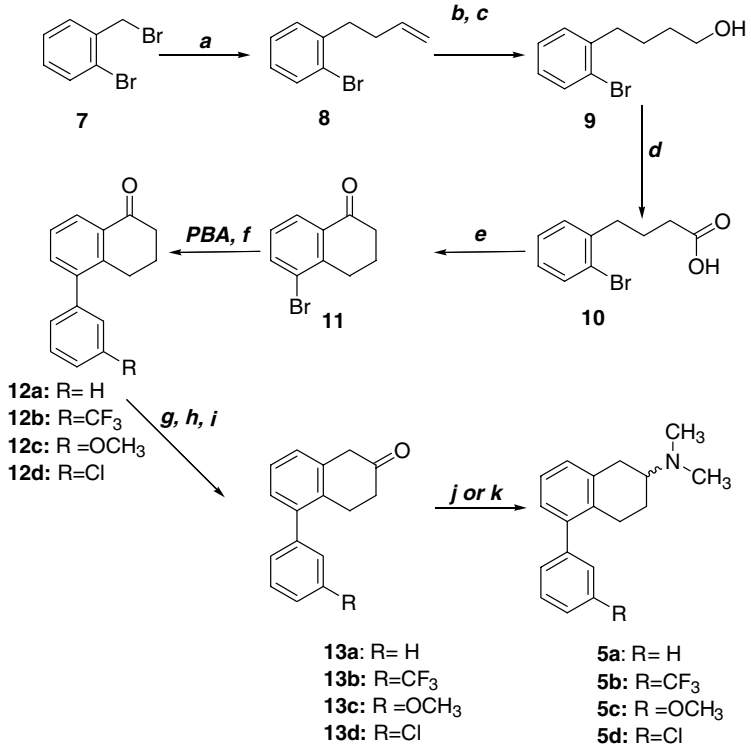


**Scheme 1.** Synthesis of 5-APT (**5a**–**d**). Reagents and conditions: Reagents and conditions: (a) allylmagnesium bromide, THF, reflux under $N_2$; (b) 0.4 M 9-BBN in hexanes, stir under $N_2$; (c) NaOH, 30% $H_2O_2$, THF, 50 °C; (d) $CrO_3$, AcOH, rt; (e) $SOCl_2$, $CS_2$, reflux; then $AlCl_3$, reflux; (f), 2 M $Na_2CO_3$, PBA, toluene, reflux; (g) $NaBH_4$, MeOH, toluene; (h) oxalic acid, reflux; (i) mCPBA, $CH_2Cl_2$, rt; then boron trifluoride diethyl etherate; (j) 4 Å molecular sieves, 2.0 M dimethylamine in MeOH, $CH_2Cl_2$, rt under $N_2$; then $NaCNBH_3$, rt; (k) 2.0 M dimethylamine in MeOH, Pd/C, $H_2$, 45 psi, rt PBA: Corresponding *m*-substituted phenylboronic acid.

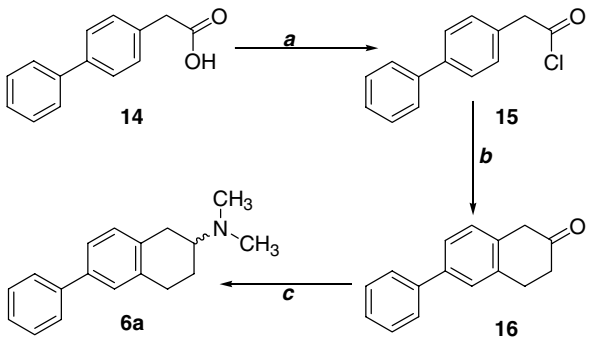


**Scheme 2.** Synthesis of 6-APT (**6a**). Reagents and conditions: (a) $SOCl_2$, benzene, rt; (b) $AlCl_3$, ethylene gas, ice bath; (c) 2.0 M dimethylamine in MeOH, acetic acid, $NaBH_3CN$, rt.

coupling of the C-3 and C-4 protons at 2.58 and 3.06 ppm, respectively, resulting in 6-phenyl-2-tetralone (**16**). Use of mildly acidic conditions (pH 5.5–6.0)[32] facilitated the reductive amination[33] of **16** via dimethylamine in the presence of sodium cyanoborohydrite as a reducing agent to give racemic 6-APT (**6a**) for initial pharmacological testing.

Scheme 3 shows several synthetic pathways to obtain the *m*-substituted 6-APTs (**6b–e**). Methods 1 and 2 used the *m*-substituted-4-biphenyl acetic acid derivatives (**20a–d**) that correspond to the 4-biphenylacetic acid (**14**) starting material in Scheme 2, however, as **20a–d** are not commercially available, these analogs were synthesized. In Method 1, esterification of 4-bromophenylacetic acid (**17**) to **18** and Suzuki–Miyaura[29] palladium-catalyzed cross-coupling gave ~80% yield of the biaryl derivatives **19a–d**, which were hydrolyzed to the corresponding *m*-substituted-4-biphenyl acetic acids **20a–d**. In Method 2, **17** was coupled with the corresponding PBA in the presence of $Pd_2$-dibenzylidene acetone $(dba)_3$ to directly produce **20a–d**, according to the method of Molander.[34] Cyclization of **20a–d** to the tetralone, followed by

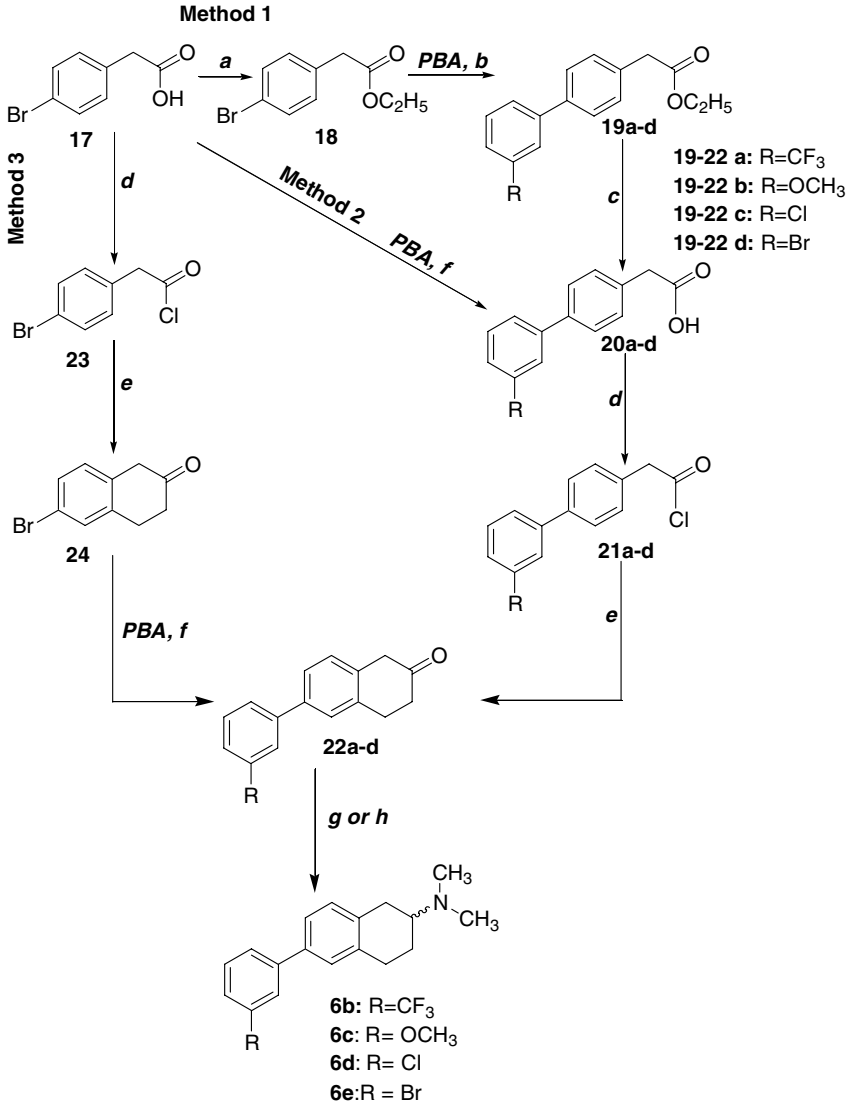


**Scheme 3.** Synthesis of *m*-halogenated-6-APTs (**6b–e**). Reagents and conditions: (a) *p*-toluenesulfonic acid, EtOH, reflux; (b) PBA, $Pd(PPh_3)_4$, $Na_2CO_3$, benzene, reflux, dark conditions; (c) 1N NaOH, reflux; (d) $SOCl_2$, rt; (e)$AlCl_3$, ethylene gas, ice bath; (f) PBA, $Pd_2(dba)_3$, $K_2CO_3$, 65 ° C, under $N_2$; (g) 2.0 M dimethylamine in MeOH, acetic acid, $NaBH_3CN$, rt; (i) 2.0 M dimethylamine in MeOH, Pd/C, $H_2$, 45 psi, rt.

reductive amination, proceeded as in Scheme 1 to provide **6b**–**e**.

In Method 3 cyclization to the tetralone was completed first, followed by coupling to the desired PBA. Thus, 6-bromo-2-tetralone (**24**) was obtained from 4-bromophenylacetic acid (**17**) as in Scheme 2. The Suzuki–Miyaura reaction directly coupled **24** to the appropriate PBA to produce the corresponding biaryl-2-tetralones (**22a**–**d**). These underwent reductive amination via sodium cyanoborohydride or catalytic hydrogenation to yield racemic *m*-substituted 6-APTs (**6b**–**e**) for initial pharmacological testing.

## 2.2. Pharmacology

**2.2.1. Affinity of APTs for human $H_1$ receptors expressed in CHO cells.** Radioreceptor competition binding assays to assess $H_1$ affinity of the APTs, in comparison to histamine, were conducted with the standard $H_1$ antagonist radioligand [$^3$H]mepyramine using membranes prepared from CHO cells stably transfected with the human $H_1$ receptor cDNA (CHO-$H_1$).[4,35] Membranes from mock-transfected CHO-K1 cells were prepared as for CHO-$H_1$ cells and selective $H_1$ antagonists also were used to verify effects observed were $H_1$ receptor-dependent. No $H_1$ radioligand specific binding was detected in membranes prepared from CHO-K1 cells ([$^3$H]mepyramine total and nonspecific saturation binding was 480 ± 49 and 460 ± 27 fmol/mg protein [mean ± SEM], respectively).

Affinity ($K_i$) values for histamine and the APTs (**5a**–**d**, **6a**–**e**) are shown in Table 1 and several representative ligand concentration–radioligand displacement curves are shown in Figure 3. Curves are sigmoidal in shape and span about 4 log-concentration units to achieve complete radioligand displacement, characteristic of competitive displacement of $\sim K_D$ radioligand concentration from a single population of GPCRs. It is noted that the modest affinity values obtained for these racemates did not warrant isomer separation for drug development purposes, however, important affinity structure–activity data from these studies are used in the computational/molecular modeling studies below to glean structural information about the $H_1$ binding pocket.

The relatively low $H_1$ affinity of the endogenous agonist histamine ($K_i \sim 13.5$ μM, Table 1) is consistent with

**Table 1.** Affinity of APT analogs for histamine $H_1$ receptors

| $H_1$ ligand | Compound | Binding affinity $K_i$ (μM) ± SEM | Hill slope $n_H$ ± SEM |
|---|---|---|---|
| Histamine | **1** | 13.5 ± 0.80 | 0.67 ± 0.01 |
| 5-APT | **5a** | 3.09 ± 0.41 | 1.12 ± 0.08 |
| $CF_3$-5-APT | **5b** | 6.27 ± 0.21 | 1.02 ± 0.08 |
| $OCH_3$-5-APT | **5c** | 3.20 ± 0.09 | 1.19 ± 0.09 |
| Cl-5-APT | **5d** | 2.65 ± 0.05 | 0.71 ± 0.08 |
| 6-APT | **6a** | 9.57 ± 0.73 | 1.18 ± 0.11 |
| $CF_3$-6-APT | **6b** | 2.74 ± 0.16 | 0.71 ± 0.07 |
| $OCH_3$-6-APT | **6c** | 1.22 ± 0.27 | 0.90 ± 0.09 |
| Cl-6-APT | **6d** | 1.31 ± 0.14 | 0.96 ± 0.06 |
| Br-6-APT | **6e** | 0.13 ± 0.01 | 1.01 ± 0.01 |

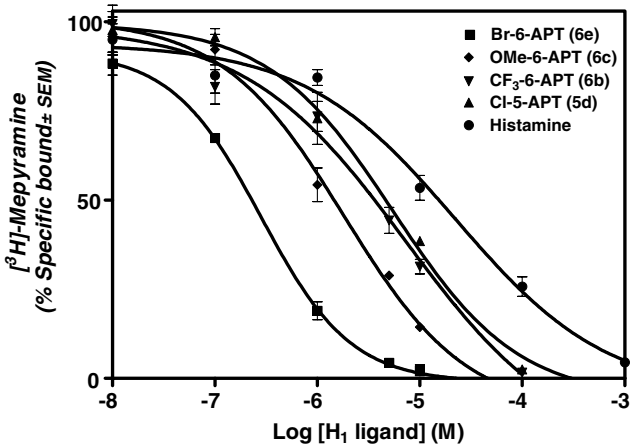


**Figure 3.** Representative $H_1$ radioligand ([$^3$H]mepyramine) displacement curves for **5d**, **6b**, **6c**, **6e**, and histamine using membranes prepared from CHO-$H_1$ cells.

results obtained previously using similar assay conditions.[35] The 5-APT series (**5a**–**d**) showed about 2 to 4 times higher $H_1$ affinity ($K_i \sim 3$–6 μM, Table 1) than histamine. Interestingly, however, the chemical nature of the *meta*-substituent of **5a**–**d** does not appear to significantly affect $H_1$ affinity, as $K_i$ values within the 5-APT series varied by only about 2-fold. In contrast, $K_i$ values among the 6-APT series (**6a**–**e**) vary by about 100-fold (0.1–10 μM, Table 1), strongly dependent on the nature of the *meta*-substituent of the pendant phenyl ring. For example, the *meta*-Br-substituted analog **6e** ($K_i \sim 0.1$ μM) has dramatically improved $H_1$ affinity compared to the parent compound 6-APT (**6a**) ($K_i \sim 10$ μM), that, in turn, is about equipotent with the endogenous agonist histamine. The other 6-APT analogs (**6b**–**d**) have $H_1$ affinity ($K_i \sim 1$–3 μM, Table 1) about midway between the parent compound **6a** and the *meta*-Br-substituted analog **6e**, regardless of the electron-donating or -withdrawing nature of the substituent. The Hill coefficients ($n_H$) given in Table 1 for the slope of the competitive displacement curves range from about 0.7 to 1. Interestingly, only Cl-5-APT (**5d**) and $CF_3$-6-APT (**6b**) have $n_H$ values similar to histamine ($n_H \sim 0.7$, Table 1), whereas, the other APTs have $n_H$ values near unity. An $n_H$ value of <1 usually is expected for agonist ligand binding at a GPCR, according to the ternary complex model with limiting availability of G-protein,[36] as is the case here for the endogenous agonist histamine. Meanwhile, an $n_H$ value of ~1 usually is expected for antagonist ligand binding at GPCRs.

**2.2.2. $H_1$ receptor-mediated stimulation of PLC/[$^3$H]IP formation in CHO-$H_1$ cells.** Activation of $H_1$ receptors by histamine is well documented to stimulate PLC activity and intracellular IP formation in a variety of cell and tissue preparations.[1,7,35] Figure 4 is representative data that show histamine likewise stimulates PLC/[$^3$H]IP formation in a concentration-dependent manner in CHO-$H_1$ cells. The Figure 4 curve spans about 4 log-dose units, consistent with a GPCR-mediated functional effect; $E_{max} = 2000 \pm 200\%$ basal control activity at 100 μM, $EC_{50} = 3.3 \pm 1.2$ μM. The Figure 4 inset shows

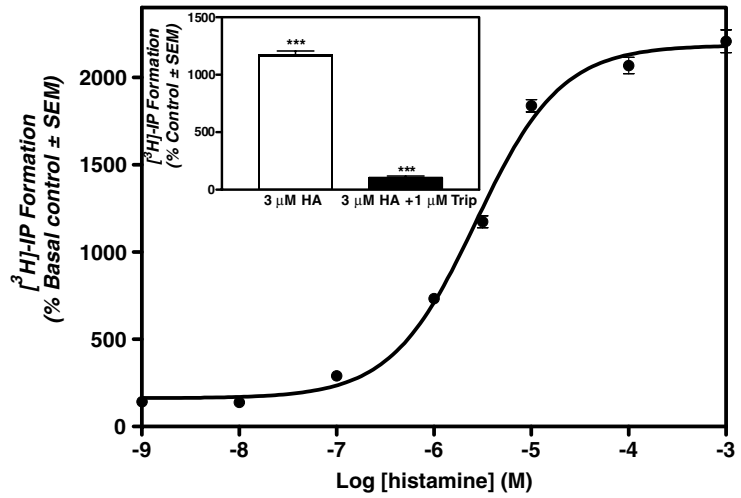


**Figure 4.** $H_1$ receptor-mediated stimulation of PLC/[$^3$H]IP formation by histamine in CHO-$H_1$ cells. Histamine $E_{max}$ = 2000 ± 200% basal control activity at 100 μM, $EC_{50}$ = 3.3 ± 1.2 μM; stimulation observed at ~$EC_{50}$ is significantly different ($^{***}t$-test $p < 0.001$) from basal control activity and is fully blocked by 1.0 μM triprolidine (inset).

that the histamine effect at $EC_{50}$ is fully blocked by the competitive $H_1$ antagonist triprolidine,[7] confirming histamine stimulation of PLC/[$^3$H]IP formation is via activation of $H_1$ receptors. In contrast, using lysates of mock-transfected CHO-K1 cells, no histamine $H_1$ receptor-mediated [$^3$H]IP formation was detected as [$^3$H]IP levels were 99 ± 1.3% basal control values (mean ± SEM) after exposure to 10 μM histamine for 15–45 min (data not shown).

At concentrations of 0.1–100.0 μM, none of the APTs produced an $H_1$-mediated concentration–response curve comparable to histamine, indicating the APTs are not agonists at $H_1$ receptors that activate PLC/IP signaling. In other experiments, it was determined that the APTs also are not agonists at $H_1$ receptors that activate AC/cAMP signaling.[37,38] Meanwhile, all the APTs in Table 1 bind to the $H_1$ receptor with higher affinity than histamine, thus, it follows that the APTs are putative $H_1$ antagonists. Characterization of the $H_1$ antagonist functional activity of only the highest affinity analog (6-Br-APT, **6e**; $K_i \sim 100$ nM, Table 1) is reported here. In these studies, histamine $H_1$-mediated stimulation of PLC/[$^3$H]IP formation was measured in the presence of increasing concentration of Br-6-APT at ~10 times (1.0 μM) and ~100 times (10 μM) its $H_1$ $K_i$ value. As shown in Figure 5, the concentration–response curve for histamine stimulation of PLC/[$^3$H]IP formation is shifted to the right in the presence of increasing concentration of Br-6-APT, indicating competitive antagonism by Br-6-APT. For these experiments, the histamine $EC_{50}$ is 1.12 ± 1.84 μM in the absence of Br-6-APT, in good

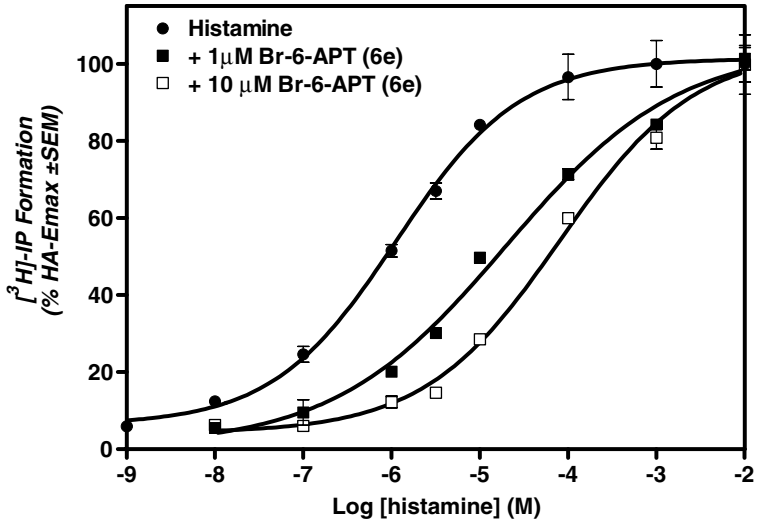


**Figure 5.** Br-6-APT competitive antagonism of $H_1$ receptor-mediated stimulation of PLC/[$^3$H]IP formation by histamine. The concentration–response curve for histamine $H_1$ receptor-mediated stimulation of PLC/[$^3$H]IP formation is shifted to the right in the presence of increasing concentration of Br-6-APT, suggesting competitive antagonism of the histamine effect by Br-6-APT. Histamine $EC_{50}$ = 0.12 ± 1.84 μM in absence of Br-6-APT; $EC_{50}$ = 19.6 ± 7.22 μM and 80.5 ± 2.91 μM, in the presence of 1.0 and 10 μM Br-6-APT, respectively (ANOVA $p < 0.0001$). These data yield an apparent $K_B$ value of 12.0 nM for Br-6-APT activity as a competitive $H_1$ receptor antagonist.

agreement with results from Figure 4. The histamine $EC_{50}$ value increases significantly (ANOVA $p < 0.0001$) to 19.6 ± 7.22 and 80.5 ± 2.91 μM, in the presence of 1.0 and 10 μM Br-6-APT, respectively. These data yield an apparent $K_B$ value of 12.0 nM for Br-6-APT activity as a competitive $H_1$ receptor antagonist. The other APTs also were able to antagonize histamine $H_1$-mediated stimulation of PLC/[$^3$H]IP formation at concentrations near their $H_1$ $K_i$ values (data not shown). Full concentration–response curves to demonstrate competitive $H_1$ antagonism were not obtained for the other APTs because their relatively low $H_1$ affinity values required concentrations of >100 μM APT analog, presenting solubility problems in this assay.

**2.2.3. Activity of APTs at human serotonin $5HT_{2A}$ and $5HT_{2C}$ receptors expressed in CHO cell membranes.** Interestingly, the human histamine $H_1$ receptor is phylogenetically most closely related to the human serotonin 5-$HT_{2A}$ and 5-$HT_{2C}$ GPCRs, versus, for example, the histamine $H_{2-4}$ GPCRs.[4,39] Here again, there is a paucity of high affinity selective (i.e., $5HT_{2C}$ over $5HT_{2A}$) agonist ligands, despite promising pharmacotherapeutic potential of $5HT_{2C}$ agonists in neuropsychiatric disorders (e.g., eating disorders, obsessive-compulsive disorder[52]). For comparison to their $H_1$ receptor activity summarized above, preliminary screening of several APTs (**5a**, **6a**, **6d**, **6e**) for activity at 5-$HT_{2A}$ and 5-$HT_{2C}$ receptors has been completed by the NIMH-sponsored Psychoactive Drug Screening Program (PDSP).[40] Results for receptor affinity are summarized in Table 2. The parent APTs (i.e., **5** and **6**) have about 5 to 10 times higher affinity for 5-$HT_{2A}$ and 5-$HT_{2C}$ receptors ($K_i$ values ~0.3–1.5 μM, Table 2) in comparison to $H_1$ receptors ($K_i$ values ~3 and 10 μM, Table 1), with 5-APT having ~2.5 times more selectivity for 5-$HT_{2C}$ over 5-$HT_{2A}$ receptors ($K_i \sim 0.3$ and 0.8 μM, respectively, Table 2). The Br-6-APT analog (**6e**), however, is in fact more selective (~5 times) for $H_1$ receptors ($K_i \sim 0.1$ μM, Table 1) than 5-$HT_{2A}$ and 5-$HT_{2C}$ receptors ($K_i \sim 0.5$ μM, Table 2). The Cl-6-APT analog (**6d**) has about equipotent affinity for $H_1$ and 5-$HT_{2A}$ receptors ($K_i \sim 1$ μM, Tables 1 and 2) and is about 5 times less active at 5-$HT_{2C}$ receptors ($K_i \sim 5$ μM, Table 2).

Similar to histamine $H_1$ receptors, serotonin 5-$HT_{2A}$ and 5-$HT_{2C}$ receptors activate PLC in CHO-$H_1$ cells.[39,41] Preliminary functional data for 5-APT (**5a**) and Cl-6-APT (**6d**) stimulation of PLC/[$^3$H]IP formation in CHO-$5HT_{2A}$ and CHO-$5HT_{2C}$ cells (provided from the PDSP[40]) are shown in Figure 6. Neither 5-APT (**5a**) nor Cl-6-APT (**6d**) activates $5HT_{2A}$ receptors. In contrast, both 5-APT (**5a**) and Cl-6-APT (**6d**) activate 5-$HT_{2C}$ receptors to stimulate PLC/[$^3$H]IP formation in a concentration-dependent manner, spanning about 4 log-dose units, consistent with a GPCR-mediated functional effect. These data suggest 5-APT ($EC_{50} \sim$ 80 nM, Fig. 6) and Cl-6-APT ($EC_{50} \sim 4$ μM, Fig. 6) are novel 5-$HT_2$ receptor agonists that selectively activate 5-$HT_{2C}$ over 5-$HT_{2A}$ receptors.

**Table 2.** Affinity of APT analogs for $5HT_{2A}$ and $5HT_{2C}$ receptors

| Ligand | Compound | Binding affinity $K_i$ (nM) ± SEM | |
|---|---|---|---|
| | | $5HT_{2A}$ | $5HT_{2c}$ |
| 5-APT | **5a** | 800 ± 100 | 310 ± 60 |
| 6-APT | **6a** | 1200 ± 300 | 1500 ± 300 |
| Cl-6-APT | **6d** | 1200 ± 200 | 4600 ± 900 |
| Br-6-APT | **6e** | 580 ± 80 | 540 ± 70 |

## 2.3. Molecular modeling

**2.3.1. 3D QSAR modeling for APT binding to $H_1$ receptors.** A CoMFA model was developed for ligand binding to the human $H_1$ receptor, including the APTs synthesized here (**5a–d** and **6a–e**, Table 1), PAT analogs previously synthesized in our laboratory[25,27,42] (**25–59**, Chart 1), and, a structurally diverse group of other commercially available $H_1$ ligands (**60–90**, Chart 2, Table 3). Common structural features of the 75 $H_1$ receptor ligands used in this study were identified using the pharmacophore mapping program DISCO[43] and the resulting alignment was utilized in CoMFA to correlate ligand steric and electrostatic fields with $H_1$ receptor affinity.

The 75 test $H_1$ ligands were separated into training and test sets. The training set consisted of compounds **5a–b**, **5d**, **6a–d**, and **25–74**, and, the test set consisted of compounds **5c**, **6e**, and **75–90**. As summarized in Table 4, the training set CoMFA resulted in a leave-one-out cross-validated correlation coefficient ($q^2$) of 0.530 and standard error of prediction (SDEP) of 0.993 (7 components); non-cross-validated partial least squares (PLS) analysis yielded a conventional $R^2$ of 0.967 and a standard error of estimate (SEE) of 0.257.

Chart 3 shows the experimental (actual) $H_1$ receptor affinity value compared to the calculated value for each compound in the training set, and, a plot of these data are shown in Figure 7, illustrating that the residuals are low. Chart 3 also shows the predicted $H_1$ affinity values for each compound in the test set and these data are plotted in Figure 8, yielding a predictive $R^2$ of 0.788, which indicates this CoMFA model has a high degree of external predictability.[44]

Figures 9A and B show the electrostatic and steric fields, respectively, for the $H_1$ receptor CoMFA model derived here. The structures of (−)-*trans*-PAT (**25**, white), $CF_3$-5-APT (**5b**, orange), and $CF_3$-6-APT (**6b**, magenta) are shown as representative ligands. The blue (favorable positive charge) and red (unfavorable positive charge) electrostatic contours in Figure 9A represent 80% and 20% level contributions, respectively. The electrostatic blue region adjacent to the amine moiety in Figure 9A indicates that a positively charged amine moiety is well-accommodated in this region of the $H_1$ receptor binding pocket. This result is consistent with previous molecular modeling studies that suggest the protonated amine moiety of $H_1$ ligands forms an ionic bond with the $Asp^{107}$ residue in transmembrane helice (TMH)-3 of the human $H_1$ receptor.[26,27] The equivalent TMH3 $Asp^{107}$ residue is highly conserved among biogenic

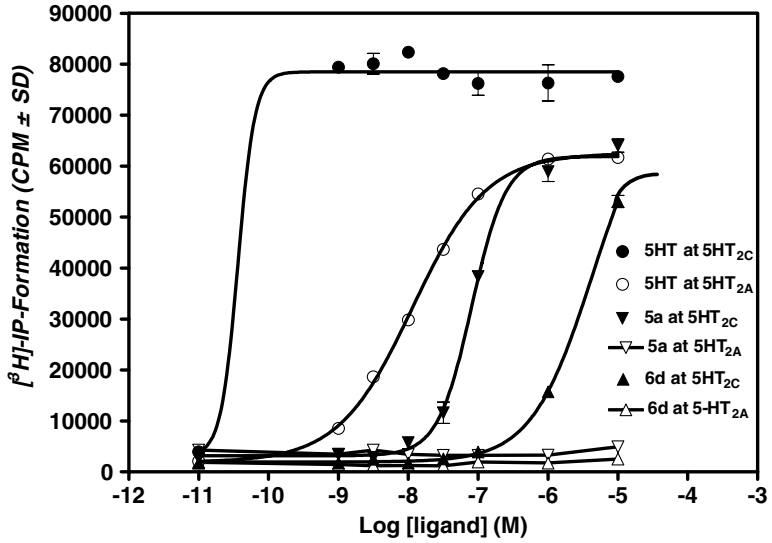


**Figure 6.** Effect of 5-APT and Cl-6-APT on $5HT_{2A}$ and $5HT_{2C}$ receptor-mediated stimulation of PLC/[$^3$H]IP formation in CHO-$H_1$ cells. Preliminary data adapted from Ref. 40. Serotonin $EC_{50} \sim 5$ nM ($5HT_{2C}$), 10 nM ($5HT_{2A}$); 5-APT (**5a**) $EC_{50} \sim 80$ nM ($5HT_{2C}$); Cl-6-APT (**6d**) $EC_{50} \sim 4$ μM ($5HT_{2C}$). Data adapted from PDSP.[40]

amine neurotransmitter GPCRs and mutagenesis studies suggest this residue interacts with a positively charged amine moiety of endogenous agonists and other ligands,[45] including for the $H_1$ receptor[46] and the serotonin $5HT_2$ receptor family[47,48] that is phylogenetically closely related to $H_1$.[4]

The green (sterically favorable) and yellow (sterically unfavorable) contours shown in Figure 9B represent 80% and 20% level contributions, respectively. The steric contour map indicates that dimethyl substitution of the amine group is sterically favorable for binding, whereas, larger substituents are unfavorable. The large yellow-colored region in the vicinity of the 5-APT pendant phenyl ring suggests the presence of this substituent is sterically unfavorable for $H_1$ receptor binding, consistent with the experimentally determined result that 5-APTs have relatively low $H_1$ affinity (Table 1). A similar negative steric interaction is associated with the pendant phenyl ring of the 6-APTs (Fig. 9B). It is noted, however, that the receptor space in the vicinity of the 6-APT phenyl ring *meta*-substituent (**6b–e**) apparently was not adequately probed given the absence of both electrostatic (Fig. 9A) and steric (Fig. 9B) fields in this region. Experimental results, however, clearly indicate $H_1$ receptor affinity of 6-APTs can vary about 100 times, depending on the nature of the pendant phenyl ring *meta* substituent (Table 1).

## 3. Discussion

Considering first the aromatic region (left side) of the structures shown in Figure 1, it is noted that introduction of a substituent at the *meta*-position of the 2-phenylhistamine benzene ring (**2a**, Fig. 1) can yield selective partial $H_1$ agonists with up to 10 times improved affinity, compared to histamine.[5,19,20] Similar substitutions at the *ortho* and *para* positions of **2**, however, result in reduced $H_1$ affinity and agonist efficacy,[5,19] suggesting an exclusive favorable steric tolerance for *meta* substituents.[50] In contrast to the 2-phenylhistamines, *meta*-Cl or *meta*-F substitution on one phenyl ring of the histaprodifen type $H_1$ agonists (**3**, Fig. 1) provides activity only about equivalent to the parent compound—it is thought that the unsubstituted diphenylpropane moiety already maximizes steric interaction with the $H_1$ binding pocket.[23] To the best of our knowledge, PATs (**4**, Fig. 1) with *meta*-substituents on the pendant phenyl moiety have not been reported.

For the 5-APTs, $H_1$ receptor affinity varied little regardless of the chemical nature of the *meta*-substituent on the pendant phenyl ring. In contrast, *meta*-substitution on the pendant phenyl moiety of 6-APT increases affinity up to 100-fold. In fact, molecular models comparing the 5- and 6-APTs to 2-phenylhistamine **2** (Fig. 2) suggest that the pendant phenyl ring of 6-APT (rather than 5-APT) more closely resembles the spatial orientation of **2** phenyl moiety. As with the 2-phenylhistamines,[5,19,20] there appears to be a combination of steric and electronic factors present in the Br-6-APT (**6e**) pendant phenyl moiety that provides enhanced $H_1$ activity, which might be improved upon using other sterically large electronegative substituents. Unfortunately, optimal electronegative, lipophilic, and steric parameters of the 6-APT*meta*-substituent cannot be determined here because the current analogs do not adequately probe the corresponding $H_1$ receptor space (absence of both electrostatic and steric fields in the pendant phenyl ring region; Fig. 9). Nevertheless, experimental affinity results (Table 1) establish that the $H_1$ receptor binding pocket interacts more substantially with the pendant phenyl ring of 6-APTs versus 5-APTs, which is important information for refining 3-D homology models of $H_1$ receptor.[22]

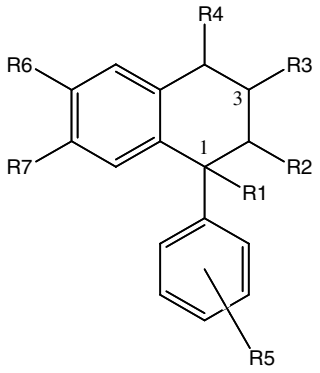


| compd | config | R1 | R2 | R3 | R4 | R5 | R6 | R7 | $K_i$ (nM) |
|---|---|---|---|---|---|---|---|---|---|
| 25 | (-)-trans | H | H | $N(CH_3)_2$ | $CH_2$ | H | H | H | 0.58 ± 0.10 |
| 26 | (+)-trans | H | H | $N(CH_3)_2$ | $CH_2$ | H | H | H | 11.5 ' ± 0.13 |
| 27 | (-)-cis | H | H | $N(CH_3)_2$ | $CH_2$ | H | H | H | 4.91 ± 0.03 |
| 28 | (+)-cis | H | H | $N(CH_3)_2$ | $CH_2$ | H | H | H | 77.7 ± 1.07 |
| 29 | (±)-trans | H | H | $N(CH_3)_2$ | $CH_2$ | H | Cl | OH | 0.63 ± 0.05 |
| 30 | (±)-trans | H | H | $N(CH_3)_3$ | $CH_2$ | H | H | H | 35 ± 2.5 |
| 31 | (±)-trans | H | H | $NH(CH_3)$ | $CH_2$ | H | H | H | 112 ± 31 |
| 32 | (±)-trans | H | H | $N(C_2H_5)_2$ | $CH_2$ | H | H | H | 5.7 ± 0.04 |
| 33 | (±)-trans | H | H | $NCH_3(C_3H_5)$ | $CH_2$ | H | H | H | 3.4 ± 0.3 |
| 34 | (±)-trans | H | H | $N(C_3H_5)_2$ | $CH_2$ | H | H | H | 10.2 ± 1.7 |
| 35 | (±)-cis | H | $N(CH_3)_2$ | H | $CH_2$ | H | H | H | 1200 ± 100 |
| 36 | (±)-trans | H | $N(CH_3)_2$ | H | $CH_2$ | H | H | H | 940 ± 53 |
| 37 | (±)-cis | H | H | $N(CH_3)_2$ | $C_2H_4$ | H | H | H | 150 ± 10.3 |
| 38 | (±)-trans | H | H | $N(CH_3)_2$ | $C_2H_4$ | H | H | H | 20.9 ± 2.4 |
| 39 | (±)-trans | H | H | $N(CH_3)_2$ | $CH_2$ | H | OH | OH | 60 ± 5.8 |
| 40 | (±)-cis | H | H | $N(CH_3)_2$ | $CH_2$ | H | OH | OH | 9.6 ± 1.7 |
| 41 | (±)-trans | $CH_3$ | H | $N(CH_3)_2$ | $CH_2$ | H | H | H | 18.3 ± 1.9 |
| 42 | (±)-cis | $CH_3$ | H | $N(CH_3)_2$ | $CH_2$ | H | H | H | 1.90 ± 0.50 |
| 43 | (±)-trans | H | H | $NCH_3((CH_2)_2C_6H_5)$ | $CH_2$ | H | H | H | 140 ± 24 |
| 44 | (±)-trans | H | H | $NCH_3((CH_2)_3C_6H_5)$ | $CH_2$ | H | H | H | 333 ± 33 |
| 45 | (±)-trans | H | H | $NCH_3((CH_2)_4C_6H_5)$ | $CH_2$ | H | H | H | 212 ± 39 |
| 46 | (±)-trans | H | H | $N(CH_3)_2$ | $CH_2$ | o -Cl | H | H | 53 ± 11.2 |
| 47 | (±)-trans | H | H | $N(CH_3)_2$ | $CH_2$ | o -$CH_3$ | H | H | 10.2 ± 1.7 |
| 48 | (±)-trans | H | H | $N(CH_3)_2$ | $CH_2$ | p -Cl | H | H | 9.0 ± 2.8 |
| 49 | (±)-trans | H | H | $N(CH_3)_2$ | $CH_2$ | p -$CH_3$ | H | H | 2.47 ± 0.23 |
| 50 | (±)-trans | H | H | $N(CH_3)_2$ | $CH_2$ | p -F | H | H | 1.53 ± 0.10 |
| 51 | (±)-cis | H | H | $N(CH_3)_3$ | $CH_2$ | H | H | H | 117 ± 2.8 |
| 52 | (±)-cis | H | H | $N(CH_3)_2$ | $CH_2$ | H | Cl | OH | 0.54 ± 0.1 |
| 53 | (±)-cis | H | H | $NH_2$ | $CH_2$ | H | OH | OH | >5000 |
| 54 | (±)-trans | H | H | $NH(CH_3)$ | $CH_2$ | H | Cl | OH | 8.1 ± 0.8 |
| 55 | (±)-trans | H | H | $NH(C_3H_5)$ | $CH_2$ | H | H | H | 45 ± 11 |
| 56 | (±)-trans | H | H | $NH(CH_2)_3C_6H_5$ | $CH_2$ | H | H | H | 2500 ± 400 |
| 57 | (±)-trans | H | H | $NH(CH_2)_4C_6H_5$ | $CH_2$ | H | H | H | 1500 ± 200 |
| 58 | (±)-trans | H | H | $NH_2$ | $CH_2$ | H | OH | OH | >5000 |
| 59 | (±)-trans | H | H | $NH_2$ | $CH_2$ | H | H | H | 1270 ± 92 |

[a] Adapted from Bucholtz et al., 1999; the R4 position is within the cyclohexyl ring

**Chart 1.** $H_1$ receptor affinity of PAT analogs[A] used in CoMFA studies. [A]Adapted from Ref. 27; the R4 position is within the cyclohexyl ring.

Turning attention to the amine (right) side of the structures shown in Figure 1, it is noted that the positively charged amine moiety of agonist and antagonist $H_1$ ligands is proposed to interact with $Asp^{107}$ in TMH3 of the $H_1$ receptor.[27,45,46] In the histaprodifen series (**3**), $N^{\alpha}$-monomethylation and $N^{\alpha}$,$N^{\alpha}$-dimethylation re-

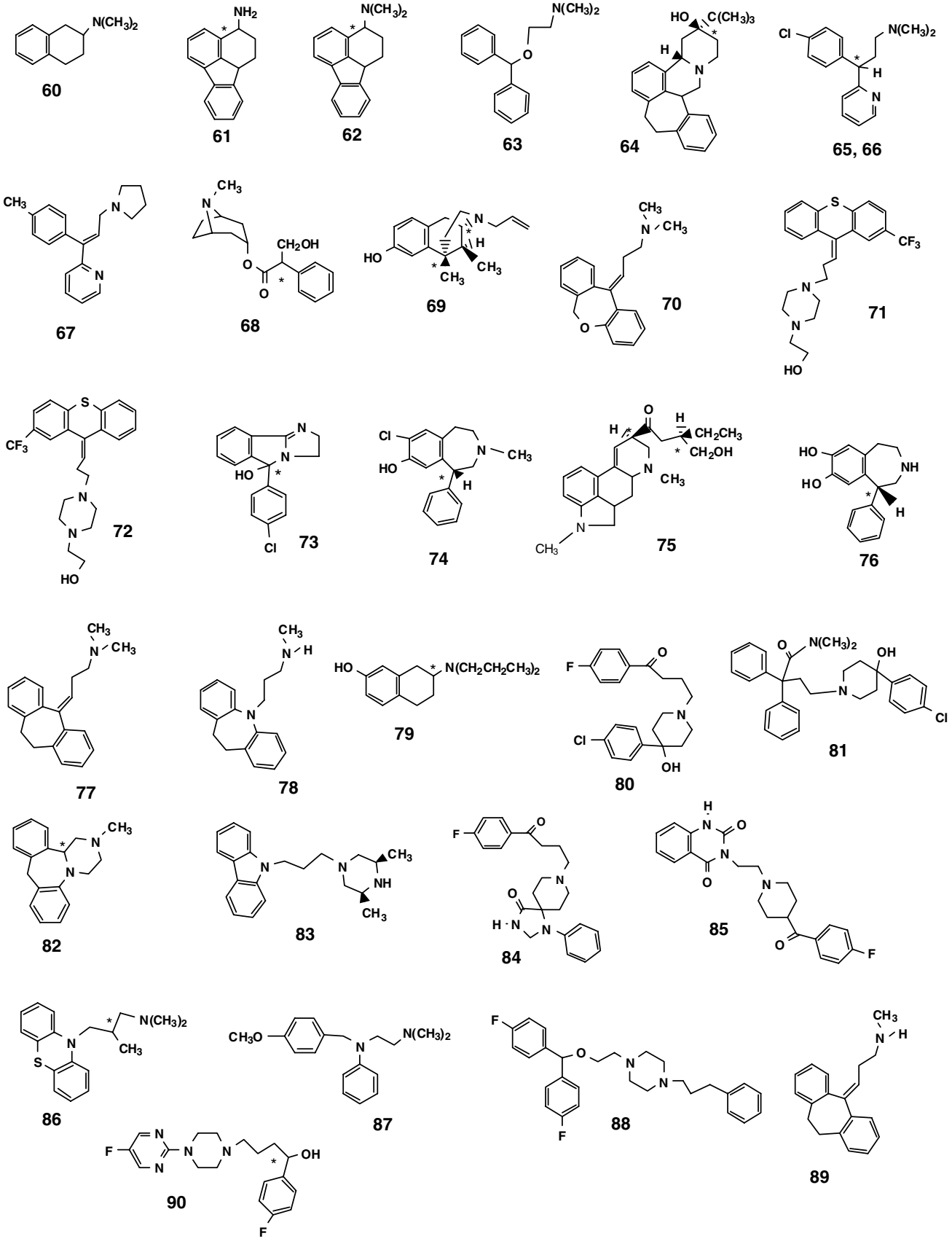


**Chart 2.** Other ligands used in CcMFA study.

**Table 3.** $H_1$ receptor affinity of other ligands[a] used in CoMFA studies

| Ligand | Compound | Binding affinity $K_i$ (nM) ± SEM |
|---|---|---|
| 2-(Dimethylamino)tetralin | **60** | 165 ± 24 |
| 3-Aminofluoranthene | **61** | ca. 4800 |
| 3-(Dimethylamino)fluoranthene | **62** | ca. 4800 |
| Diphenhydramine | **63** | 9.57 ± 0.79 |
| (+)-Butaclamol | **64** | 147 ± 13 |
| (*R*)-Chlopheniramine | **65** | 80.0 ± 7.4 |
| (*S*)-Chlopheniramine | **66** | 0.31 ± 0.03 |
| Tripolidine | **67** | 0.69 ± 0.07 |
| Atropine | **68** | 1240 ± 177 |
| (−)-NANM | **69** | > 5000 |
| Doxepin | **70** | 0.16 ± 0.02 |
| *cis*-Flupenthixol | **71** | 0.86 ± 0.17 |
| *trans*-Flupenthixol | **72** | 5.73 ± 0.85 |
| Mazindol | **73** | ca. 600 |
| SCH-23390 | **74** | 101 ± 14 |
| Methylsergide | **75** | ca. 3000 |
| SKF-38393 | **76** | ca. 2500 |
| Amytriptyline | **77** | 0.50 ± 0.03 |
| Desipramine | **78** | 45.4 ± 1.8 |
| 7-OH-DPAT | **79** | ca. 1500 |
| Haloperidol | **80** | 215 ± 20 |
| Loperamine | **81** | ca. 2000 |
| Mianserin | **82** | 0.30 ± 0.07 |
| Rimcazole | **83** | >5000 |
| Spiperone | **84** | 272 ± 48 |
| Ketanserin | **85** | 1.79 + 0.05 |
| Promethazine | **86** | 0.24 ± 0.06 |
| Mepyramine | **87** | 0.74 ± 0.05 |
| GBR-12909 | **88** | 9.33 ± 1.66 |
| Nortryptyline | **89** | 15.1 ± 5.6 |
| (±)-BMY-1402 | **90** | 180 ± 14 |

[a] Adapted from Ref. 27.

**Table 4.** Summary of CoMFA results

| | Training set[a] |
|---|---|
| Optimal no. of components | 7 |
| $q^2$ | 0.530 |
| SDEP | 0.993 |
| SEE | 0.257 |
| $R^2$ | 0.967 |
| *F* value | 202.874 |
| Prob of $R^2 = 0$ | 0.000 |
| Relative contributions steric | 0.605 |
| Electrostatic | 0.395 |

[a] Compounds **5a**–**b**, **5d**, **6a**–**d**, **25**–**74**.

sults in about 5-times higher $H_1$ affinity, compared to histamine.[5] Likewise, amine moiety dimethylation for the PAT series (**4**) provides optimal $H_1$ affinity, compared to monomethyl, trimethyl, and, larger alkyl, dialkyl, and aryl substituents.[25,27,42] Moreover, an analogous dimethylamine moiety is common to many clinically effective, high-affinity, $H_1$ antagonists (e.g., chlorpheniramine, diphenhydramine).[13] It follows then that dimethyl substitution of the APT amino group likely is already optimal. Meanwhile, stereochemistry of APT amino moiety may be expected to influence both $H_1$ receptor affinity and functional activity, especially in view of results reported for PAT isomers.[35,51] For example, the *trans*-(1*R*,3*S*)-(−)-PAT isomer displays highest

| | | training set[a] | | test set[b] | |
|---|---|---|---|---|---|
| compd | actual | calcd | resid | pred | resid |
| **5a** | 5.81 | 5.50 | 0.31 | | |
| **5b** | 5.50 | 5.60 | -0.10 | | |
| **5c** | 5.80 | | | 5.60 | 0.20 |
| **5d** | 5.88 | 6.24 | -0.36 | | |
| **6a** | 5.32 | 5.63 | -0.31 | | |
| **6b** | 5.86 | 5.97 | -0.11 | | |
| **6c** | 6.22 | 6.23 | -0.01 | | |
| **6d** | 6.19 | 5.91 | 0.28 | | |
| **6e** | 7.18 | | | 6.63 | 0.55 |
| **25** | 9.24 | 9.00 | 0.24 | | |
| **26** | 7.94 | 8.03 | -0.09 | | |
| **27** | 8.31 | 8.39 | -0.08 | | |
| **28** | 7.11 | 7.23 | -0.12 | | |
| **29** | 9.46 | 8.91 | 0.55 | | |
| **30** | 7.76 | 8.39 | -0.63 | | |
| **31** | 7.25 | 6.84 | 0.41 | | |
| **32** | 8.55 | 8.69 | -0.14 | | |
| **33** | 8.77 | 8.81 | -0.04 | | |
| **34** | 8.26 | 8.30 | -0.04 | | |
| **35** | 6.22 | 6.89 | -0.07 | | |
| **36** | 6.33 | 6.57 | -0.24 | | |
| **37** | 7.26 | 6.83 | 0.43 | | |
| **38** | 7.98 | 7.90 | 0.08 | | |
| **39** | 7.52 | 7.55 | -0.03 | | |
| **40** | 8.32 | 8.34 | -0.02 | | |
| **41** | 8.04 | 8.00 | -0.09 | | |
| **42** | 9.02 | 8.06 | -0.02 | | |
| **43** | 7.15 | 6.94 | 0.21 | | |
| **44** | 6.78 | 6.85 | -0.07 | | |
| **45** | 6.97 | 7.14 | -0.17 | | |
| **46** | 7.58 | 7.30 | 0.28 | | |
| **47** | 8.29 | 8.53 | -0.24 | | |
| **48** | 8.35 | 8.77 | -0.42 | | |
| **49** | 8.85 | 8.86 | 0.17 | | |
| **50** | 9.12 | 8.68 | 0.44 | | |
| **51** | 7.23 | 7.18 | 0.05 | | |
| **52** | 9.60 | 9.61 | -0.01 | | |
| **53** | 5.30 | 5.69 | -0.39 | | |
| **54** | 8.38 | 8.54 | -0.16 | | |
| **55** | 7.35 | 6.96 | 0.39 | | |
| **56** | 5.90 | 5.75 | 0.15 | | |
| **57** | 6.12 | 6.23 | -0.11 | | |
| **58** | 5.30 | 5.58 | -0.28 | | |
| **59** | 6.20 | 6.61 | -0.41 | | |
| **60** | 7.08 | 6.98 | 0.10 | | |
| **61** | 5.32 | 5.22 | 0.10 | | |
| **62** | 5.32 | 5.07 | 0.25 | | |
| **63** | 8.02 | 7.96 | 0.06 | | |
| **64** | 6.83 | 7.17 | -0.34 | | |
| **65** | 7.10 | 7.07 | 0.03 | | |
| **66** | 9.51 | 9.34 | 0.17 | | |
| **67** | 9.16 | 9.31 | -0.15 | | |
| **68** | 5.91 | 5.85 | 0.06 | | |
| **69** | 5.30 | 5.10 | 0.20 | | |
| **70** | 9.80 | 9.81 | -0.01 | | |
| **71** | 9.07 | 9.20 | -0.13 | | |
| **72** | 8.24 | 8.15 | 0.09 | | |
| **73** | 7.04 | 7.03 | 0.01 | | |
| **74** | 7.00 | 6.98 | 0.02 | | |
| **75** | 5.52 | | | 4.72 | 0.80 |
| **76** | 5.60 | | | 5.39 | 0.21 |
| **77** | 9.30 | | | 8.43 | 0.87 |
| **78** | 7.34 | | | 7.94 | -0.60 |
| **79** | 5.82 | | | 5.90 | -0.08 |
| **80** | 6.67 | | | 6.95 | -0.28 |
| **81** | 5.70 | | | 5.67 | 0.03 |
| **82** | 9.52 | | | 7.87 | 1.65 |
| **83** | 5.30 | | | 6.16 | -0.86 |
| **84** | 6.57 | | | 6.09 | 0.48 |
| **85** | 8.75 | | | 8.95 | -0.20 |
| **86** | 9.62 | | | 8.27 | 1.35 |
| **87** | 9.13 | | | 8.56 | 0.57 |
| **88** | 8.03 | | | 8.53 | -0.50 |
| **89** | 7.82 | | | 6.49 | 1.33 |
| **90** | 6.74 | | | 6.53 | 0.21 |

[a] compounds **5a-b, 5d, 6a-d, 25-74**. [b] compounds **5c, 6e, 75-90.**

**Chart 3.** CoMFA results and predicted $H_1$ affinity ($-\log[K_i]$) for ligands in training and test sets.

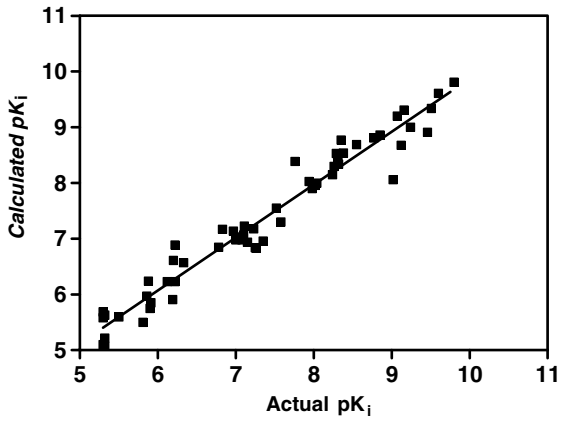


**Figure 7.** Actual versus calculated $H_1$ receptor p$K_i$ values for the training set (**5a**–**b**, **5d**, **6a**–**d**, and **25**–**74**) using CoMFA (cf. Table 4).

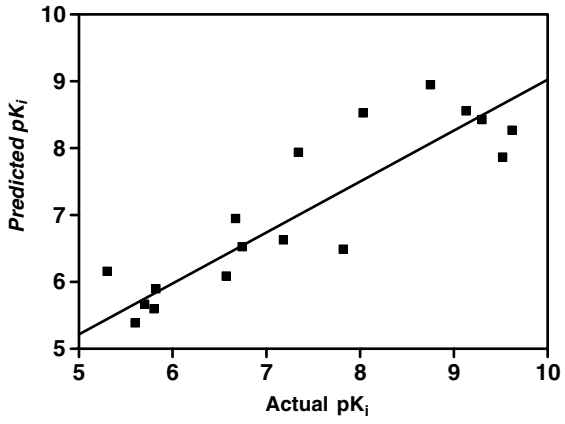


**Figure 8.** Actual versus predicted $H_1$ receptor p$K_i$ values for the test set (**5c**, **6e**, and **75**–**90**) using CoMFA (cf. Table 4); $R^2 = 0.788$.

$H_1$ affinity ($K_i \sim 1$ nM), while the corresponding *trans*-(1*S*, 3*R*)-(+)-PAT enantiomer has about 20 times lower affinity. Meanwhile, $H_1$ affinity of the *cis*-PAT enantiomers is several times lower than their corresponding *trans*-PAT diastereomers, with *cis*-(1*S*, 3*S*)-(−)-PAT ($K_i \sim 5$ nM) having about 15 times higher affinity than *cis*-(1*R*, 3*R*)-(+)-PAT.[35] Taken together, these results indicate that stereochemistry at especially the C3 (amino) position of PAT (i.e., *S* configuration shared by both [−]-*trans*- and [−]-*cis*-PAT) is an important molecular determinant for binding to the $H_1$ receptor. Accordingly, it is predicted that the *S*-enantiomers of the (*R*, *S*)-APTs reported here will show 2 times higher $H_1$ affinity as compared to the racemates. It is noted, however, that even for the highest affinity analog, (*R*, *S*)-Br-6-APT (**6d**), the *S*-isomer is predicted to have a $K_i$ value of about 50 nM—not impressive compared to clinically used $H_1$ receptor competitive antagonists such as triprolidine that has a $K_i$ value of about 1.0 nM.[7]

Although $H_1$ agonist functional activity was not observed for the APTs, CoMFA modeling results summarized in Figure 9 provide a correlation of APT molecular structure parameters that result in differential $H_1$ binding interactions—such interactions form the molecular basis for $H_1$ receptor activation. Also, implicit in the CoMFA results is ligand-based information that can be used to help predict structural features of the $H_1$ active site. In this regard, the more structurally rigid APT and PAT analogs, as compared to flexible 2-phenylhistamine and histaprodifen-type $H_1$ ligands, should be more effective templates to define the 3-D arrangement of $H_1$ active site amino acid residues involved in ligand binding and function.

Previously, a CoMFA-based 3-D QSAR with a high degree of internal predictability[44] ($q^2 = 0.67$) was developed for $H_1$ receptor ligands, including PATs.[27] Using this CoMFA model, $H_1$ receptor affinity was predicted to be relatively high for the 5-APTs (i.e., $K_i \sim 20$–60 nM) and relatively low for the 6-APTs (i.e., $K_i \sim 600$–2000 nM). In fact, the experimentally determined $K_i$ values are about 2-log units higher than predicted for the 5-APTs and about 1-log unit higher for the 6-APTs (Table 1). To develop a more predictive QSAR here, a CoMFA model first was developed for a training set of $H_1$ ligands. This model then was used to predict affinity values for an external test set of ligands.[44] Using this approach, models that yield $q^2 > 0.5$ for the training set and $R^2 > 0.6$ for the test

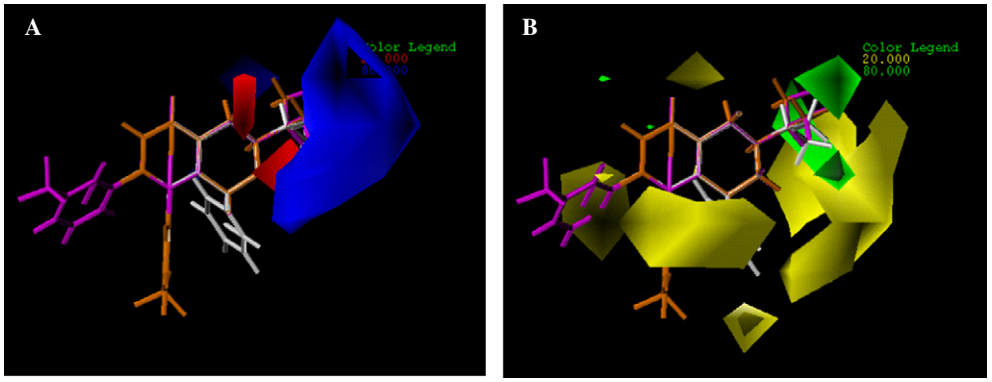


**Figure 9.** CoMFA electrostatic and steric stdev * coeff contour plots. Representative ligands are (−)-*trans*-PAT (**25**, white), $CF_3$-5-APT (**5b**, orange), and $CF_3$-6-APT (**6b**, magenta). (A) Electrostatic contour plots. Blue regions represent a contribution level of 80%, that is, favorable positive charge areas. Red regions represent a contribution level of 20%, that is, unfavorable positive charge areas. (B) Steric contour plots. Green regions represent a contribution level of 80%, that is, sterically favorable areas. Yellow regions represent a contribution level of 20%, that is, sterically unfavorable areas.

set indicate a QSAR with higher internal and external predictive power versus 'traditional' CoMFA.[44] Thus, the $H_1$CoMFA model obtained here ($q^2 = 0.530$; $R^2 = 0.788$) predicts $H_1$ ligand binding with a higher degree of external predictability compared to the previously reported model ($q^2 = 0.67$).[27] The current study did not include enough analogs to robustly probe the 6-APT pendant phenyl ring *meta* substituent binding space. Current results suggest, however, that such 6-APT (but not 5-APT) derivatives likely will provide useful information about $H_1$ receptor structure and function in view of affinity values that vary about 100 times, depending on the nature of the 6-APT*meta* substituent. The primary importance of the 6-APT*meta* (rather than *ortho* and *para*) substituent found here is consistent with studies of **2a**[5,19–21] and the 6-APT/**2** molecular model presented in Figure 2B. Meanwhile, the 5-APT pendant phenyl ring (regardless of substitution) apparently occupies a space that is sterically unfavorable for $H_1$ receptor binding, highlighting the significance of the misalignment of phenyl rings for 5-APT and **2** shown in Figure 2A.

## 4. Summary

APT-type molecular features that confer $H_1$ receptor affinity may be predicted from the current 3-D QSAR results. In general, the APT molecular scaffold is suitable to provide $H_1$ competitive antagonist functional activity but not $H_1$ agonism. Development of selective $H_1$ receptor agonists continues to be hampered by limited 3-D structural details for the GPCR superfamily, and, the apparently subtle molecular mechanisms that govern GPCR activation.[49] On the other hand, the APTs reported here offer promise regarding design of agonists for the serotonin $5HT_{2C}$ GPCR. Preliminary results (Table 2 and Fig. 6) indicate 5-APT (**5a**) and Cl-6-APT (**6d**) bind to and selectively activate $5HT_{2C}$ receptors. Moreover, $5HT_{2C}$ functional potency of 5-APT ($EC_{50} \sim 80$ nM) is about 3 times higher than its $5HT_{2C}$ affinity ($K_i \sim 300$ nM), suggesting efficient receptor activation. Thus, (*R*,*S*)-5-APT (**5a**) is about 2 times greater than (*S*)-2-(5,6-difluoroindol-1-yl)-1-methylethylamine ($EC_{50} \sim 200$ nM),[53] previously, one of the most potent and selective $5HT_{2C}$ agonists yet identified. Accordingly, further medicinal chemical studies of the lipophilic (brain-penetrating) APT molecular scaffold may yield potent $5HT_{2C}$ agonists with pharmacotherapeutic potential in neuropsychiatric diseases.

## 5. Experimental

### 5.1. CHO cell human $H_1$ receptor transfection and culture

Chinese hamster ovary cells deficient in dihydrofolate reductase (CHO-K1) were stably transfected with the guinea pig histamine $H_1$ receptor cDNA.[54] Clonal transfects expressing the $H_1$ receptor (CHO-$H_1$) were selected for in α-minimal essential media without ribonucleosides and supplemented with 10% fetal bovine serum and 2 mM L-glutamine. For binding and functional studies, CHO-$H_1$ cells were grown to 90% confluence in 75 $cm^2$ tissue culture flasks containing α-minimum essential medium, supplemented with 10% fetal bovine serum, 2 mM L-glutamine, and 0.1% penicillin–streptomycin (100 U/100 μg/ml), in a humidified atmosphere of air/$CO_2$ (95:5%) at 37 °C.

Null-transfected CHO-K1 cells were cultured as above and used to verify that effects observed were $H_1$receptor-dependent (selective $H_1$ antagonists also were used). Essentially, no $H_1$ radioligand specific binding was detected in membranes prepared from CHO-K1 cells as [$^3$H]mepyramine total and nonspecific saturation binding was $480 \pm 49$ and $460 \pm 27$ fmol/mg protein (mean ± SEM), respectively. Also, essentially no histamine receptor-mediated IP or cAMP second messenger formation was detected in lysates of CHO-K1 cells as second messenger levels were $99 \pm 1.3$% basal control values (mean ± SEM) after exposure to 10 μM histamine for 15–45 min.

### 5.2. Radioreceptor assays

Radioligand competition binding assays were performed using membrane homogenate prepared from CHO-$H_1$ cells, as previously reported.[7,35] Membranes were incubated with $\sim K_D$ concentration of the standard $H_1$ antagonist radioligand [$^3$H]mepyramine (1.0 nM), plus, test ligand (10nM–300 μM), in 50 mM $Na^+$–$K^+$ phosphate buffer (total assay volume was 0.4 ml) for 30 min at 25 °C. Non-specific binding was defined with triprolidine (10 μM). Inhibition data were analyzed by nonlinear regression using the sigmoidal curve-fitting algorithm in Prism 3.0 (Graphpad, San Diego, CA) to determine $IC_{50}$ and Hill coefficient ($n_H$). Ligand affinity is expressed as an approximation of $K_i$ values using the equation, $K_i = IC_{50}/1 + L/K_D$, where $L$ is the concentration of radioligand having affinity $K_D$.[55] Each experimental condition was run in triplicate and each experiment was performed a minimum of three times to determine SEM.

### 5.3. Measurement of [$^3$H]inositol phosphate formation in CHO-$H_1$ cells

Formation of [$^3$H]inositol phosphates ([$^3$H]IP) was measured in CHO-$H_1$ cells, as described previously.[35] Briefly, CHO-$H_1$ cells were incubated overnight in 12-well culture plates (ca. $7.0 \times 10^4$ cells/well) with [$^3$H]myo-inositol (0.4 μCi), a precursor of the PLC-β substrate phosphatidylinositol. Aliquots of drug stocks were added in triplicate in the presence of 50 mM LiCl (total well volume = 0.5 ml) and incubation continued at 37 °C for 45 min. After aspiration of media, wells were placed on ice and lysed by incubation with 50 mM formic acid (15 min). Formic acid was neutralized with ammonium hydroxide and well contents were added to individual AG1-X8 200–400 formate resin anion exchange columns. Ammonium formate/formic acid (1.2 M/0.1 M) was used to elute [$^3$H]IP directly into scintillation vials for counting of tritium. Resulting data were analyzed using the nonlinear regression algorithm in Prism 3.0, and are expressed as mean percent control [$^3$H]IP

formation, and potencies are expressed as concentrations required to produce 50% maximal [$^3$H]IP formation ($EC_{50}$) ± SEM ($n \geqslant 3$).

### 5.4. Molecular modeling

SYBYL (version 6.6; Tripos Associates, St. Louis, MO) molecular modeling software was used for structure generation and CoMFA.[56] Default SYBYL settings were used except where otherwise noted. Structure optimization and field fit minimization were performed using the standard Tripos force field with the maximum iteration cutoff of 1000 steps. SYBYL random search method was used to search for low energy conformers. All calculations were performed on a Silicon Graphics Indigo2 workstation.

**5.4.1. Structure generation and alignment rules.** $H_1$ receptor affinity values ($K_i$) were determined for 75 chemically diverse ligands, including the 5- and 6-APTs synthesized here (**5a–d** and **6a–e**, Table 1), PAT analogs previously synthesized in our laboratory[25,27,42] (**25–59**, Chart 1), and, a structurally diverse group of other commercially available $H_1$ ligands (**60–90**, Chart 2, Table 3). Common structural features of the 75 $H_1$ receptor ligands used in this study were identified using the pharmacophore mapping program DISCO[43] and the resulting alignment was utilized in CoMFA to correlate ligand steric and electrostatic fields with $H_1$ receptor affinity. Ligand affinity is expressed as $-\log(K_i)$. For chiral compounds, the isomer structure corresponding most closely to the (1*R*, 3*S*)-(−)-*trans*-PAT template molecule was modeled and affinity approximated by using one-half the $K_i$ value of the racemate.[27,35]

The template molecule (1*R*, 3*S*)-(−)-*trans*-PAT (**25**) and compounds **26–90** were modeled as described in a previous CoMFA modeling study of the PAT binding site.[27] The APTs (*S*-configuration to match the template molecule) were constructed de novo using the sketch option of the SYBYL building component. Conformational databases for the APTs were generated using the SYBYL Systematic Search routine using 5° increments to rotate the pendant phenyl ring, with a maximum energy cutoff of 10 kcal/mol above the lowest-energy conformer. The SYBYL field fit routine was used to align the APT conformers with the template molecule, matching the protonated nitrogen and the centroid of the aromatic portion of the tetralin ring. The five lowest energy conformers of the APTs were systematically aligned to the template to determine the conformations that provided the highest $q^2$.

**5.4.2. Comparative molecular field analysis.** Conventional CoMFA[56] was performed with the QSAR option of SYBYL. A grid with spacing 2.0 Å between closest points was built in the *x*, *y*, and *z* dimensions within the region defined by the aligned molecules. It extended beyond the van der Waals envelopes of all molecules by at least 4.0 Å. Steric and electrostatic field energies in each grid point were calculated using sp$^3$carbon probe atoms with +1 charge. PLS algorithm as implemented in SYBYL was used to build CoMFA models for the training set (compounds **5a–b**, **5d**, **6a–d**, and **25–74**). If steric or electrostatic energy values for some grid points had variations lower than 2.0 (minimum $\sigma$ value), they were excluded from the calculations. The optimal number of principal components in the final PLS model was determined by the standard error of prediction value obtained from the leave-one-out cross-validation technique. The non-cross-validated CoMFA model was built with the optimal number of principal components. It was used to predict $H_1$ affinity of the test set compounds (**5c**, **6e**, and **75–90**). To represent favorable and unfavorable areas for steric and electrostatic contributions, 80% and 20% stdev * coeff contour plots were built.

### 5.5. Syntheses

Reagents and solvents were obtained in highest available purity from Sigma–Aldrich (Milwaukee, WI) or Fisher Scientific (Hampton, NH). Column chromatography was performed with 60 Å silica gel (70–230 mesh). $^1$H NMR spectra were obtained in $CDCl_3$ using a Varian VXR 300 MHz instrument with shifts reported in parts per million (ppm) relative to trimethylsilane (TMS). Mass spectra were measured using an Agilent 1100 instrument with LC/MSD trap or LCQ Deca ion trap. Elemental analyses were performed by Atlantic Microlab, Inc. (Norcross, GA) and are within ±0.4% of calculated values unless otherwise noted. Melting points were determined on a Mel-temp apparatus and are uncorrected.

**5.5.1. 4-(*o*-Bromophenyl)-1-butene (8).** 2-Bromophenylbromide (11.8 g; 0.0472 mol) in dry THF was cooled in an ice bath under an atmosphere of nitrogen. Following dropwise addition of 1.0 M allylmagnesium bromide in ether, the mixture was refluxed for 1.5 h. After cooling to room temperature, the mixture was placed in an ice bath and quenched by addition of 2 M $H_2SO_4$. Water was added to dissolve all solids and the aqueous layer was extracted with ether. The combined organic layers were dried over $Na_2SO_4$, filtered and concentrated in vacuo to afford a yellow liquid (9.29 g, 94% yield); $^1$H NMR: $\delta$ 7.55 (d, 1H), 7.2–7.26 (m, 2H), 7.0–7.1 (m, 1H), 5.8–5.95 (m, 1H), 4.95–5.1 (m, 2H), 2.78–2.86 (m, 2H), 2.3–2.4 (m, 2H).

**5.5.2. 4-(*o*-Bromophenyl)-butanol (9).** 9-Borabicyclo[3.3.1]nonane (BBN) (0.4 M) in hexanes (9 mL) was added dropwise to 8 (0.509 g; 0.0024 mol) under nitrogen. The mixture was stirred at room temperature until all starting material was consumed (18 h), as indicated by TLC. Following addition of 6 M NaOH (0.4 mL), THF (1 mL), and 30% $H_2O_2$ (0.9 mL), the mixture was heated at 50 °C for 1.5 h. After cooling, the layers were separated. The organic layer was washed sequentially with saturated $NaHSO_3$, water, and brine. The aqueous extracts were combined, saturated with potassium carbonate, filtered, and extracted with ether. Organic fractions were combined, dried over $Na_2SO_4$, filtered, and concentrated in vacuo to afford a yellow oil (457.3 mg, 82% yield); $^1$H NMR: $\delta$ 7.5 (d, 1H), 7.18–7.21 (m, 2H), 7.01–7.1 (m, 1H), 3.64 (t, 2H), 2.75 (t, 2H), 1.6–1.75 (m, 2H), 1.4–1.6 (m, 2H).

**5.5.3. 4-(*o*-Bromophenyl)-butyric acid (10).** A solution of chromium trioxide (9.8 g; 0.0980 mol) in 90% acetic acid (100 mL) was added dropwise to 9 (10.02 g; 0.0437 mol) at 0 °C, then stirred for 18 h at room temperature. After dilution with water, the mixture was extracted with ether, washed with water and brine, and extracted with 2 M NaOH. The aqueous layer was acidified to pH 3 with $H_2SO_4$, then extracted with ether. The ether portions were combined, dried over $Na_2SO_4$, filtered, and concentrated to afford a yellow liquid. Recrystallization from ether afforded white crystals (5.63 g, 58% yield); mp 84–87 °C (lit.[57] 88–89 °C), $^1$H NMR: $\delta$ 7.55 (d, 1H), 7.2–7.3 (m, 2H), 7.0–7.1 (m, 1H), 2.75–2.85 (t, 2H), 2.35–2.45 (t, 2H), 1.9–2.05 (m, 2H).

**5.5.4. 5-Bromo-1-tetralone (11).** In thionyl chloride (10 mL; 0.133 mol), 10 (0.938 g; 0.0038 mol) was dissolved and refluxed for 45 min. After cooling, excess thionyl chloride was removed and the residue dissolved in carbon disulfide (10 mL; 0.166 mol). After gradual addition of aluminum chloride (0.77 g; 0.0057 mol), the mixture was refluxed for 3 h. Once cooled to room temperature, 75% HCl (cold) was added and the mixture was extracted with ethyl acetate. The organic layer was dried over $Na_2SO_4$, filtered, and concentrated in vacuo. Recrystallization from hexanes afforded white crystals (540 mg, 57% yield); mp 48–51 °C (lit.[58] 49–50 °C), $^1$H NMR: $\delta$ 8.0 (d, 1H), 7.7 (d, 1H), 7.15–7.25 (t, 1H) 3.0 (t, 2H), 2.65 (t, 2H), 2.1–2.2 (m, 2H).

**5.5.5. General procedure for preparation of 5-(*m*-substituted)-phenyl-1-tetralones (12a–d).** The following were combined and refluxed for 24 h in the dark: **11** (1.95 g; 0.0086 mol) in toluene (10 mL), tetrakis(triphenylphosphine)palladium (0) $Pd(PPh_3)_4$, 0.277 g; 0.00023 mol in toluene (10 mL), 2 M $Na_2CO_3$ (8 mL), and, the appropriate *m*-substituted phenylboronic acid (PBA, 0.0103 mol) in EtOH (10 mL). After cooling, 30% $H_2O_2$ (1.2 mL) was added to oxidize residual phenylboronic acid. The mixture was stirred at room temperature for 1 h and then extracted with ether. The organic layer was washed with brine, dried over $Na_2SO_4$, filtered, and concentrated. Purification via column chromatography (eluent: hexanes) afforded **12a**–**d** as solids (24–86% yield).

**5.5.5.1. 5-Phenyl-1-tetralone (12a).** (1.96 g, 86% yield, white solid) Mp 97–101 °C (lit.[59] 103–105 °C), $^1$H NMR: $\delta$ 8.05 (d, 1H), 7.2–7.5 (m, 7H), 2.85 (t, 2H), 2.65 (t, 2H), 2.02 (m, 2H).

**5.5.5.2. 5-(*m*-Trifluoromethylphenyl)-1-tetralone (12b).** (2.06 g, 69% yield, yellow solid) Mp 114–118 °C, $^1$H NMR: $\delta$ 8.05 (d, 1H), 7.4–7.65 (m, 6H), 2.8 (t, 2H), 2.6 (t, 2H), 2.05 (m, 2H).

**5.5.5.3. 5-(*m*-Methoxyphenyl)-1-tetralone (12c).** (0.623 g, 24% yield, yellow solid) Mp 115–120 °C, $^1$H NMR: $\delta$ 8.1 (d, 1H), 7.2–7.65 (m, 6H), 3.85 (s, 3H), 2.85 (t, 2H), 2.65 (t, 2H), 2.05 (m, 2H).

**5.5.5.4. 5-(*m*-Chlorophenyl)-1-tetralone (12d).** (1.53 g, 58% yield, yellow solid) Mp 115–120 °C, $^1$H NMR: $\delta$ 8.05 (d, 1H), 7.2–7.5 (m, 6H), 2.85 (t, 2H), 2.65 (t, 2H), 2.02 (m, 2H).

**5.5.6. General procedure for preparation of 5-(*m*-substituted)-phenyl-2-tetralones (13a–d).** A solution of the corresponding 5-(*m*-substituted)-phenyl-1-tetralone (**12a**–**d**, 0.00046 mol) in dry toluene was added dropwise to a suspension of $NaBH_4$(0.250 g, 0.0066 mol) in dry MeOH under nitrogen. The mixture was warmed to room temperature, two volumes of water were added, and, the mixture was stirred for 1 h. The organic layer was separated, dried over $Na_2SO_4$, filtered, and solvent removed in vacuo to afford the tetralols as yellow oils (90–100% yields). *5-Phenyl-1-tetralol* (0.092 g, 90% yield); $^1$H NMR: $\delta$ 7.1–7.7 (m, 8H), 4.85 (t, 1H), 2.45–2.7 (m, 2H), 1.6–2.1 (m, 4H). *5-(m-Trifluoromethylphenyl)-1-tetralol* (0.134 g, 100% yield.); $^1$H NMR: $\delta$ 7.1–7.65 (m, 7H), 4.85 (t, 1H), 2.45–2.7 (m, 2H), 1.7–2.1 (m, 4H). *5-(m-Methoxyphenyl)-1-tetralol* (0.117 g, 100% yield.); $^1$H NMR: $\delta$ 7.5 (d, 1H), 6.8–7.4 (m, 6H), 4.85 (t, 1H), 2.5–2.7 (m, 2H), 1.7–2.1 (m, 4H). *5-(m-Chlorophenyl)-1-tetralol* (0.119 g, 100% yield.); $^1$H NMR: $\delta$ 7.0–7.7 (m, 7H), 4.75 (s, 1H), 2.3–2.6 (m, 2H), 1.7–1.9 (m, 4H).

The tetralols (0.00077 mol) were stirred and heated to reflux for 5 h in 20% aqueous oxalic acid. After cooling to room temperature, the mixture was diluted with one volume water and extracted with ether. The aqueous layer was re-extracted with ethyl acetate and the combined organic extracts were dried over $Na_2SO_4$, filtered, and concentrated in vacuo to afford the alkenes as oils (61–74% yield). *8-Phenyl-1,2-dihydronaphthalene* (0.117 g, 74% yield, yellow oil); $^1$H NMR: $\delta$ 7.0–7.5 (m, 8H), 6.5 (d, 1H), 6.05 (m, 1H), 2.7 (t, 2H), 2.2 (m, 2H). **8**-(*m-Trifluoromethylphenyl)-1,2-dihydronaphthalene* (0.152 g, 72% yield, colorless oil); $^1$H NMR: $\delta$ 7.5–7.7 (m, 5H), 7.25 (t, 1H), 7.15 (m, 1H), 6.6 (d, 1H), 6.1 (m, 1H), 2.7 (t, 2H), 2.5 (m, 2H). *8-(m-Methoxyphenyl)-1,2-dihydronaphthalene* (0.129 g, 71% yield, colorless oil); $^1$H NMR: $\delta$ 7.0–7.4 (m, 5H), 6.85–6.95 (m, 2H), 6.55 (d, 1H), 6.1 (m, 1H), 3.8 (s, 3H), 2.75 (t, 2H), 2.2 (m, 2H). *8-(m-Chlorophenyl)-1,2-dihydronaphthalene* (0.113 g, 61% yield, Brown oil); $^1$H NMR: $\delta$ 7.0–7.5 (m, 7H), 6.5 (d, 1H), 6.05 (m, 1H), 2.7 (t, 2H), 2.2 (m, 2H).

*m*-Chloroperoxybenzoic acid (0.339 g; 0.0019 mol) was added, with stirring, to a solution of the alkenes (0.84 mmol) in $CH_2Cl_2$(5 mL) at 0 °C. After stirring for 30 min, the mixture was washed in succession with 25% sodium metabisulfite, saturated $NaHCO_3$, and water. The organic layer was dried over $Na_2SO_4$ and filtered. $BF_3$-etherate (0.06 mL) was added to the filtrate at 0 °C. The mixture was shaken briefly, then, allowed to stand at room temperature for 5 min. The solution was washed successively with water and saturated $NaHCO_3$. The organic layer was dried over $Na_2SO_4$, filtered, and dried in vacuo. Purification via column chromatography (eluent: 95% $CH_2Cl_2$, 5% methanol) afforded the 2-tetralones (**13a**–**d**) as yellow oils (30–54% yield).

**5.5.6.1. 5-Phenyl-2-tetralone (13a).** (0.078 g, 42% yield.) $^1$H NMR: $\delta$ 7.1–7.5 (m, 8H), 3.65 (s, 2H), 3.05 (t, 2H), 2.4 (t, 2H).

**5.5.6.2. 5-(*m*-Trifluoromethylphenyl)-2-tetralone (13b).** (0.088 g, 36% yield.) $^1$H NMR: $\delta$ 7.5–7.7 (m, 5H), 7.1–7.35 (m, 2H), 3.65 (s, 2H), 3 (t, 2H), 2.45 (t, 2H).

**5.5.6.3. 5-(*m*-Methoxyphenyl)-2-tetralone (13c).** (0.114 g, 54% yield.) $^1$H NMR: $\delta$ 7.15–7.4 (m, 5H), 6.85–7.0 (m, 2H), 3.85 (s, 3H), 3.65 (s, 2H), 3.05 (t, 2H), 2.45 (t, 2H).

**5.5.6.4. 5-(*m*-Chlorophenyl)-2-tetralone (13d).** (0.065 g, 30% yield) $^1$H NMR: $\delta$ 7.1–7.5 (m, 7H), 3.65 (s, 2H), 3.05 (t, 2H), 2.4 (t, 2H).

**5.5.7. 2-Dimethylamino-5-phenyl-1,2,3,4-tetrahydronaphthalene (5a).** In $CH_2Cl_2$ (5 mL), **13a** (0.203 g; 0.0009 mol) and 2.0 M dimethylamine in methanol (0.5 ml) were stirred over 4 Å molecular sieves in a nitrogen atmosphere for 6 h. Previous experience is that the molecular sieves provide sufficient Lewis acidity to catalyze reductive amination. Thus, sodium cyanoborohydride (0.740 g, 0.0117 mol) was added and the mixture stirred for 17 h. After addition of 10% HCl (20 mL), the solution was filtered and extracted with ether. The aqueous layer was adjusted to pH > 10 via NaOH, then, extracted with ether and dried over $Na_2SO_4$, filtered, and dried in vacuo to afford the free base as a yellow oil. The hydrochloride salt was formed with ethereal HCl. Recrystallization in chloroform/cyclohexane provided a white powder (38.4 mg, 15% yield). Free base $^1$H NMR: $\delta$ 7.1–7.4 (m, 8H), 2.6–3.26 (m, 5H), 2.3 (s, 6H), 2.0 (m, 1H), 1.5 (m, 1H). HCl salt mp 226–230 °C (dec). $^1$H NMR: $\delta$ 7.1–7.4 (m, 8H), 3.3–3.6 (m, 2H), 3.2 (m, 2H), 3.15 (m, 1H), 2.8 (s, 6H), 2.4 (m, 1H), 1.9 (m, 1H). MS *m*/*z*: 252 $(M+H)^+$. Anal. ($C_{18}H_{21}N$·HCl·0.5 $H_2O$) C, H, N.

**5.5.8. General procedure for preparation of 2-dimethylamino-5-(*m*-substituted)-phenyl-1,2,3,4-tetrahydronaphthalenes (5b–d).** The appropriate 2-tetralone (0.00093 mol, **13b–d**) in chloroform (2 mL), 2.0 M dimethylamine in methanol (24 equiv), and, 5% Pd/C were shaken on a Parr hydrogenation apparatus at 45 psi for 18 h. The reaction mixture was filtered through Celite, adjusted to pH < 2 via 10% HCl, and, extracted with ether. The aqueous layer was adjusted to pH > 10 via NaOH, extracted with ether, dried over $Na_2SO_4$, filtered, and evaporated in vacuo to afford the free bases as yellow oils. The hydrochloride salt was prepared using ethereal HCl. Recrystallization in chloroform/cyclohexane provided white solids (15–23% yield).

**5.5.8.1. 2-Dimethylamino-5-(*m*-trifluoromethylphenyl)-1,2,3,4-tetrahydronaphthalene (5b).** (0.051 g, 17% yield) Free base $^1$H NMR: $\delta$ 7.45–7.65 (m, 4H), 7.15–7.3 (m, 2H), 7.1 (d, 1H), 2.6–3.1 (m, 5H), 2.35 (s, 6H), 2.1 (m, 1H), 1.5 (m, 1H). HCl salt: mp 95–198 °C, $^1$H NMR: $\delta$ 7.45–7.7 (m, 4H), 7.1–7.3 (m, 3H), 3.2–3.6 (m, 5H), 3.85 (t, 6H), 2.45 (m, 1H), 1.8 (m, 1H); MS *m*/*z*: 343 $(M+Na)^+$. Anal. ($C_{19}H_{20}NF_3$·HCl·0.25 $H_2O$) C, H, N, F.

**5.5.8.2. 2-Dimethylamino-5-(*m*-methoxyphenyl)-1,2,3,4-tetrahydronaphthalene (5c).** (0.060 g, 23% yield) Free base $^1$H NMR: $\delta$ 7.05–7.4 (m, 4H), 6.8–6.95 (m, 3H), 3.8 (s, 3H), 2.6–3.1 (m, 5H), 2.35 (s, 6H), 2.1 (m, 1H), 1.5 (m, 1H). HCl salt: mp 193–196 °C, $^1$H NMR: $\delta$ 7.1–7.4 (m, 4H), 6.75–6.95 (m, 3H), 3.85 (s, 3H), 3.2–3.6 (m, 5H), 3.85 (s, 6H), 2.4 (m, 1H), 1.8 (m, 1H); MS *m*/*z*: 282 $(M+H)^+$. Anal. ($C_{19}H_{23}NO$·HCl·0.75 $H_2O$) C, H, N.

**5.5.8.3. 2-Dimethylamino-5-(*m*-chlorophenyl)-1,2,3,4-tetrahydronaphthalene (5d).** (0.039 g, 15% yield) Free base $^1$H NMR: $\delta$ 7.0–7.4 (m, 7H), 2.5–3.1 (m, 5H), 2.35 (s, 6H), 2.1 (m, 1H), 1.5 (m, 1H). HCl salt: mp 194–196 °C, $^1$H NMR: $\delta$ 7.1–7.4 (m, 7H), 3.15–3.6 (m, 5H), 3.85 (t, 6H), 2.45 (m, 1H), 1.85 (m, 1H); MS *m*/*z*: 286 $(M+H)^+$.

**5.5.9. 4-Biphenyl acetyl chloride (15).** Thionyl chloride (9 mL; 124 mol) was added to a solution of 4-biphenylacetic acid (10.0 g; 0.047 mol) in benzene (25 mL) and dimethylformamide (0.1 mL). After stirring for 5 h at room temperature, the solution was concentrated in vacuo to afford the crude acid chloride **15** as a yellow hygroscopic powder (10.51 g, 97% yield); mp 47–50 °C (lit.[31] 48 °C), $^1$H NMR: $\delta$ 4.20 (s, 2H), 7.22–7.66 (m, 9H).

**5.5.10. 6-Phenyl-2-tetralone (16).**[31] An ice-cold slurry of aluminum chloride (12.9 g; 0.097 mol) in dry $CH_2Cl_2$ (150 mL) was stirred for 20 min in a 3-necked flask. A stream of dry ethylene gas was introduced and **15** (9.9 g, 0.043 mol) in $CH_2Cl_2$ (50 mL) was added dropwise over 30 min. The ethylene gas stream was continued for an additional 30 min, then the dark red mixture was stirred for 2 h at 0–10 °C. Water (100 mL) was added slowly and the mixture extracted with $CH_2Cl_2$ (200 mL). The extracts were washed with water, dried over $Na_2SO_4$, filtered, and evaporated. Purification by column chromatography (toluene or $CH_2Cl_2$) afforded the 2-tetralone **16** as a yellowish brown oil (4.2 g, 44% yield); $^1$H NMR: $\delta$ 2.58–2.63 (t, 2H), 3.06–3.12 (t, 2H), 3.61 (s, 2H), 7.2–7.6 (m, 8H).

**5.5.11. 2-Dimethylamino-6-phenyl-1,2,3,4-tetrahydronaphthalene (6a).**[60] A methanolic solution of dimethylamine (2 M in MeOH, 10.2 mL) was added dropwise over 15 min to a solution of **16** (3.3 g; 0.015 mol) in MeOH (50 mL) with stirring at 0 °C. The color of the reaction mixture turned immediately bluish green. Glacial acetic acid (1 mL; 0.017 mol) was then added and the color turned deep brown. The reaction mixture was stirred for 24 h at room temperature, then a solution of sodium cyanoborohydride (1.44 g; 0.023 mol) in MeOH (10 mL) was added and stirring continued for 48 h. The reaction was quenched and acidified to pH 2 by addition of 1 N HCl, then extracted with $Et_20$. The aqueous layer was separated, brought to pH 10 with 1 N KOH, and extracted with $Et_20$ (3× 20 mL). The combined ethereal extracts were dried over $Na_2SO_4$, filtered, and concentrated in vacuo. Column chromatography ($CH_2Cl_2$/MeOH 9:1) gave the **6a** free base as a colorless oil (0.490 g, 13% yield); $^1$H NMR: $\delta$ 2.18–2.20 (m, 2H), 2.39 (s, 6H), 2.62–2.68 (t, 2H), 2.85–2.90 (m, 1H), 3.00–3.05 (d, 2H), 7.15–7.60 (m, 8H). The free base was converted to the corresponding

hydrochloride salt by addition of ethereal HCl (10 mL). The mixture was cooled for 4 h and solvent removed in vacuo. The resulting solid was recrystallized in $CHCl_3$/hexanes to give the **6a** HCl as an off-white powder; mp 222–225 °C. $^1$H NMR: $\delta$ 1.95 (m, 1 H), 2.55–2.62 (m, 2H), 2.85 (s, 6H), 3.02–3.18 3.10 (t, 2H), 3.36–3.40 (d, 2H), 3.45–3.58 (t, 2H), 7.20–7.60 (m, 8H); MS *m*/*z*: 252.2 $(M+H)^+$. Anal. ($C_{18}H_{21}N{\cdot}HCl{\cdot}0.25\ H_2O$) C, H, N.

### 5.5.12. Preparation of 6-(*m*-substituted)-phenyl-2-tetralone (22a–d) by method 1

**5.5.12.1. Ethyl 4-bromophenylacetate (18).** A solution of **17** (14.0 g; 0.0650 mol) in absolute EtOH (150 mL) was stirred at room temperature for 15 min. *p*-Toluenesulfonic acid (0.12 g, 0.0065 mol) was added and the mixture was heated under reflux for 7 h. After cooling, the solvent was removed in vacuo and the resulting yellow liquid was dissolved in ether (100 mL). This solution was washed in succession with water, 5% $NaHCO_3$, and 5% $Na_2S_2O_3$ (3× 50 mL each), then dried over $Na_2SO_4$, filtered, and concentrated in vacuo to afford (13.2 g, 84% yield) of **18** as colorless, shiny, hygroscopic crystals; mp 31–34 °C (lit.[61] 30 °C), $^1$H NMR: $\delta$ 1.22–1.27 (t, 3H), 3.55 (s, 2H), 4.11–4.18 (q, 2H), 7.14–7.46 (m, 4H).

**5.5.12.2. General procedure for preparation of ethyl (*m*-substituted)-4-biphenylacetate (19a–d).** A solution of **18** (6 g; 0.0250 mol) in benzene (30 mL) was stirred in the dark for 15 min at room temperature. A solution of $Pd(PPh_3)_4$ (0.0866 g; 0.00075 mol) in benzene (10 mL) was added, followed by 2 M $Na_2CO_3$ (25 mL). The appropriate PBA (28 mmol) in EtOH (15 mL) was added dropwise over 20 min and the mixture was heated at reflux for 8 h. 30% $H_2O_2$ (1.5 mL) was added and the solution stirred at room temperature for 30 min to oxidize excess PBA. The mixture was extracted with ether, washed with water and brine, dried over $Na_2SO_4$, filtered, and concentrated in vacuo. The crude product was purified by column chromatography in toluene to yield the corresponding ethyl (*m*-substituted)-4-biphenylacetates **19a–d** (75–81% yield) as colorless oils.

*Ethyl (m-trifluoromethyl)-4-biphenylacetate (**19a**).* (6.24 g; 81% yield) $^1$H NMR: $\delta$ 1.25–1.30 (t, 3H), 3.66 (s, 2H), 4.14–4.21 (q, 2H), 7.24–7.81 (m, 8H).

*Ethyl (m-methoxy)-4-biphenylacetate (**19b**).* (5.40 g, 80% yield) $^1$H NMR: $\delta$ 1.25–1.30 (t, 3H), 3.66 (s, 2H), 3.85 (s, 3H), 4.14–4.21 (q, 2H), 6.87–7.57 (m, 8H).

*Ethyl (m-chloro)-4-biphenylacetate (**19c**).* (5.15 g; 75% yield) $^1$H NMR: $\delta$ 1.24–1.30 (t, 3H), 3.62 (s, 2H), 4.17 4.22 (q, 2H), 7.21–7.78 (m, 8H); MS *m*/*z*: 274.0 ($M^+$).

*Ethyl (m-bromo)-4-biphenylacetate (**19d**).* (6.14 g; 77%yield) $^1$H NMR: $\delta$ 1.24–1.30 (t, 3H), 3.60 (s, 2H), 4.13–4.21 (q, 2H), 7.17–7.70 (m, 8H).

**5.5.12.3. General procedure for preparation of *m*-(substituted)-4-biphenylacetic acids (20a–d).** A solution of the appropriate biphenylacetate (**19a–d**, 0.020 mol) in EtOH (15 mL) was stirred for 15 min at room temperature, followed by addition of 1 N NaOH (40 mL). The cloudy mixture was heated under reflux for 1 h until it became clear. After cooling to room temperature the mixture was diluted with water and extracted with ether. The aqueous layer was adjusted to pH 2–3 and re-extracted with $CHCl_3$. The organic extract was dried over $Na_2SO_4$, filtered, and concentrated in vacuo to afford the corresponding acids as white powders.

*m-(Trifluoromethyl)-4-biphenylacetic acid (**20a**).* (4.76 g; 85% yield) Mp 94–97 °C, $^1$H NMR: $\delta$ 3.72 (s, 2H), 7.25–7.82 (m, 8H). MS *m*/*z*: 279.0 (M−1).

*m-(Methoxy)-4-biphenylacetic acid (**20b**).* (4.11 g; 85% yield) Mp 91–95 °C, $^1$H NMR: $\delta$ 3.70 (s, 2H), 3.85 (s, 3H), 6.78–7.58 (m, 8H).

*m-(Chloro)-4-biphenylacetic acid (**20c**).* (3.99 g, 81% yield) Mp 125–127 °C (lit.[62] 129–131 °C), $^1$H NMR: $\delta$ 3.75 (s, 2H), 7.25–7.60 (m, 8H).

*m-(Bromo)-4-biphenylacetic acid (**20d**).* (86% yield) Mp 78–81 °C, $^1$H NMR: $\delta$ 3.60–3.75 (s, 2H), 7.16–7.78 (m, 8H).

**5.5.12.4. General procedure for preparation of acid chlorides (21a–d).** Compounds **21a–d** were synthesized from **20a–d** following the same procedure described for the preparation of **15**. Compounds **21a–d** were obtained as yellow to reddish brown oils (85–94% yield) and used without further purification. Representative $^1$H NMR (**21b**): $\delta$ 3.85 (s, 3H), 4.20 (s, 2H), 6.82–7.60 (m, 8H).

**5.5.12.5. General procedure for preparation of 6-(*m*-substituted)-phenyl-2-tetralones (22a–d).** Compounds **22a–d** were synthesized from **21a–d** following the same procedure described for the preparation of **16**. Compounds **22a–d** were obtained as yellowish brown oils. All 2-tetralones were stored under nitrogen and used within 24 h to avoid decomposition.

*6-(m-Trifluoromethylphenyl)-2-tetralone (**22a**).* (32% yield) $^1$H NMR: $\delta$ 2.58–2.62 (t, 2H), 3.16–3.18 (t, 2H), 3.62 (s, 2H), 7.20–8.18 (m, 7H).

*6-(m-Methoxyphenyl)-2-tetralone (**22b**).* (35% yield) $^1$H NMR: $\delta$ 2.57–2.62 (t, 2H), 3.14–3.18 (t, 2H), 3.60 (s, 2H), 3.85 (s, 3H), 6.88–7.50 (m, 7H).

*6-(m-Chlorophenyl)-2-tetralone (**22c**).* (40% yield) $^1$H NMR: $\delta$ 2.57–2.62 (t, 2H), 3.13–3.18 (t, 2H), 3.63 (s, 2H), 7.20–7.60 (m, 7H).

*6-(m-Bromophenyl)-2-tetralone (**22d**).* (37% yield) $^1$H NMR: $\delta$ 2.58–2.60 (t, 2H), 3.08–3.10 (t, 2H), 3.61–3.63 (s, 2H), 7.05–7.88 (m, 7H).

### 5.5.13. Preparation of 6-(*m*-substituted)-phenyl-2-tetralones (22a, b) by method 2

**5.5.13.1. *m*-(Substituted)-4-biphenylacetic acids (20a, b).** A mixture of 4-bromophenylacetic acid (0.430 g; 0.002 mol), the appropriate PBA (2.0 mmol), $K_2CO_3$ (0.829 g; 0.006 mol), and tris(dibenzylideneace-

tone)dipalladium (0) (0.018 g; 0.02 mmol, 1 mol%) was kept under nitrogen for 15–20 min at room temperature. Water (6 mL) was added via a syringe to the closed system. The reaction mixture was heated at 65 °C with stirring for 2 h. After cooling to room temperature, the mixture was filtered, treated with 1 N HCl (until pH 3–4), extracted with $CH_2Cl_2$, washed with water, and, dried over $Na_2SO_4$ and concentrated in vacuo to yield the desired biphenyl carboxylic acids (**20a**, **b**) (81–85% yield). Characterization of **20a** and **20b** was as for method 1 and the products were used to synthesize **22a** and **22b**, respectively, as in method 1.

### 5.5.14. Preparation of 6-(*m*-substituted)-phenyl-2-tetralone (22a, b) by method 3

**5.5.14.1. 4-Bromophenylacetyl chloride (23).** Compound **23** was synthesized from **17** following the same procedure described for the preparation of **15**. Compound **23** was obtained as a reddish brown oil (88% yield) and was used without further purification; $^1$H NMR: $\delta$ 4.20 (s, 2H), 7.20–7.60 (m, 4H).

**5.5.14.2. 6-Bromo-2-tetralone (24).** Compound **24** was synthesized from **23** following the same procedure described for the preparation of **16**. Compound **24** was obtained as an amber crystalline solid (54% yield); mp 66–70 °C (lit.[63] no mp reported), $^1$H NMR: $\delta$ 2.66–2.70 (t, 2H), 3.16–3.20 (t, 2H), 3.65 (s, 2H), 7.0–7.4 (m, 3H).

**5.5.14.3. General procedure for preparation of 6-(*m*-substituted)-phenyl-2-tetralones (22a, b).** Compounds **22a**, **b** were synthesized from **24**, as for **20a**, **b** in method 2. The products **22a**, **b** were obtained as yellow-brown oils and characterization was identical to the compounds obtained by methods 1 and 2.

**5.5.15. 2-Dimethylamino-6-(*m*-trifluoromethylphenyl)-1,2,3,4-tetrahydronaphthalene (6b).** Compound **6b** was synthesized from **22a** using the same procedure as described for the preparation of **5b–d**. The **6b** free base was obtained as a colorless oil (31% yield); free base $^1$H NMR: $\delta$ 2.14–2.20 (m, 2H), 2.39 (s, 6H), 2.62–2.73 (t, 2H), 2.83–2.95 (m, 1H), 2.99–3.05 (d, 2H), 7.05–7.85 (m, 7H). The oil was converted to the HCl salt, as described, for use in pharmacological studies. HCl salt: white powder, mp 177–179 °C, $^1$H NMR: $\delta$ 1.95 (m, 1 H), 2.58–2.63 (m, 2H), 2.85 (s, 6H), 3.05–3.20 (t, 2H), 3.38–3.42 (m, 1H), 3.45–3.52 (d, 2H), 7.05–7.85 (m, 7H); MS *m*/*z*: 320.2 $(M + H)^+$. Anal. ($C_{19}H_{20}F_3N\cdot$HCl) C, H, N; C: calc., 64.13. Found: 65.08, 65.10.

**5.5.16. Dimethylamino-6-(*m*-methoxy)-phenyl-1,2,3,4-tetrahydronaphthalene (6c).** Compound **6c** was synthesized from **22b** using the same procedure as described for the preparation of **5b–d**. The **6c** free base was obtained as a colorless oil (29% yield.); free base $^1$H NMR: $\delta$ 2.14–2.20 (m, 2H), 2.39 (s, 6H), 2.60–2.68 (t, 2H), 2.80–2.85 (m, 1H), 2.90–3.00 (d, 2H,), 3.85 (s, 3H), 6.87–7.57 (m, 7H). The oil was converted to the HCl salt, as described, for use in pharmacological studies. HCl salt: yellow powder, mp 165–168 °C, $^1$H NMR: $\delta$ 1.95 (m, 1 H), 2.58–2.63 (m, 2H), 2.85 (s, 6H), 3.05–3.20 (t, 2H), 3.38–3.42 (m, 1H), 3.45–3.52 (d, 2H), 3.85 (s, 3H), 6.78–7.57 (m, 7H); MS *m*/*z*: 282.4 $(M+H)^+$.

**5.5.17. 2-Dimethylamino-6-(*m*-chlorophenyl)-1,2,3,4-tetrahydronaphthalene (6d).** Compound **6d** was synthesized from **22c** using the same procedure described for **6a**. The **6d** free base was obtained as a yellow oil (17% yield); $^1$H NMR: $\delta$ 2.18–2.22 (m, 2H), 2.39 (s, 6H), 2.62–2.73 (t, 2H), 2.83–2.85 (m, 1H), 2.99–3.05 (d, 2H,), 7.15–7.60 (m, 7H). The oil was converted to the HCl salt, as described, for use in pharmacological studies. HCl salt: white powder, mp 207–210 °C, $^1$H NMR: $\delta$ 1.95 (m, 1 H), 2.55–2.65 (m, 2H), 2.85 (s, 6H), 2.95–3.20 (t, 2H), 3.22–3.38 (m, 1H), 3.42–3.50 (d, 2H), 7.15–7.60 (m, 7H); MS *m*/*z*: 285.4 $(M+H)^+$. Anal. ($C_{18}H_{20}ClN\cdot$HCl$\cdot$0.25 $H_2O$) C, H, N, Cl.

**5.5.18. 2-Dimethylamino-6-(*m*-bromophenyl)-1,2,3,4-tetrahydronaphthalene (6e).** Compound **6e** was synthesized from **22d** using the same procedure described for **6a**. The **6e** free base was obtained as a yellow oil (15% yield); $^1$H NMR: $\delta$ 2.18–2.25 (m, 2H), 2.39 (s, 6H), 2.62–2.73 (t, 2H), 2.80–.2.95 (m, 1H), 2.98–3.15 (d, 2H), 7.00–7.80 (m, 7H). The oil was converted to the HCl salt, as described, for use in pharmacological studies. HCl salt: buff-brown powder, mp 155–158 °C, $^1$H NMR: $\delta$ 1.95 (m, 1 H), 2.55–2.65 (m, 2H), 2.85 (s, 6H), 2.95–3.20 (t, 2H), 3.22–3.38 (m, 1H), 3.42–3.50 (d, 2H), 7.00–7.80 (m, 7H); MS *m*/*z*: 348 $(M^+ + H_2O)$, 330.1 $(M+H)^+$. Anal. ($C_{18}H_{20}BrN\cdot$HCl$\cdot$1.50 $H_2O$) C, H, N; Br: calcd, 20.29. Found, 21.24.

## Acknowledgments

This work was supported by United States Public Health Service Grant MH068655. The authors thank Dr. Bryan Roth (NIMH-sponsored Psychoactive Drug Screening Program) for providing preliminary affinity and functional data for activity of some APTs at several relevant CNS receptors.

## References and notes

1. Hill, S. J.; Genellin, C. R.; Timmerman, H.; Schwartz, J. C.; Shankley, N. P.; Young, J. M.; Schunack, W.; Levi, R.; Haas, H. L. *Pharmacol. Rev.* **1997**, *49*, 253–287.
2. Yamashita, M.; Ito, S.; Sugama, K.; Fukui, H.; Smith, B.; Nakanishi, K.; Wada, H. *Biochem. Biophys. Res. Commun.* **1991**, *177*, 1233–1239.
3. De Backer, M. D.; Gommeren, W.; Moereels, H.; Nobels, G.; Van-Gompel, P.; Leysen, J. E.; Luyten, W. H. *Biochem. Biophys. Res. Commun.* **1993**, *197*, 1601–1608.
4. Smit, M. J.; Hoffmann, M.; Timmerman, H.; Leurs, R. *Clin. Exp. Allergy* **1999**, *29*(Suppl. 3), 19–28.
5. Seifert, R.; Wenzel-Steifert, K.; Bürckstümmer, T.; Pertz, H. H.; Schunack, W.; Dove, S.; Buschauer, A.; Elz, S. *J. Pharmacol. Exp. Ther.* **2003**, *305*, 1104–1115.
6. Moniri, N. H.; Booth, R. G. *Soc. Neurosci. Abstr.* **2003**, *28*, 52.18.
7. Moniri, N. H.; Covington-Strachan, D.; Booth, R. G. *J. Pharmacol. Exp. Ther* **2004**, *311*, 274–281.
8. Fleckenstein, A. E.; Lookingland, K. J.; Moore, K. E. *Naunyn-Schmiedeberg's Arch. Pharmacol.* **1993**, *327*, 50–54.

9. Booth, R. G.; Owens, C. E.; Brown, R. L.; Bucholtz, E. C.; Lawler, C. P.; Wyrick, S. D. *Brain Res.* **1999**, *837*, 95–105.
10. Choksi, N. Y.; Nix, W. B.; Wyrick, S. D.; Booth, R. G. *Brain Res.* **2000**, *852*, 151–160.
11. Marley, P. D.; Robotis, R. *J. Auton. Nerv. Syst.* **1998**, *70*, 1–9.
12. Moniri, N. H.; Booth, R. G. *Soc. Neurosci. Abstr.* **2002**, *28*, 830.13.
13. Zhang, M. Q., Leurs, R., Timmerman, H. Histamine H1-receptor antagonists. In *Burgers Medicinal Chemistry and Drug Discovery*, 5th ed.; Wolff, M. E., Ed.; John Wiley: New York, 1997; Vol. 5, pp 495–559.
14. Baldessarini, R. J. Drugs and the treatment of psychiatric disorders: depression and anxiety disorders. In *The Pharmacological Basis of Therapeutics*, 10th ed.; Hardman, J. G., Limbird L. E., Gilman, A. G., Eds.; McGraw-Hill: New York, 2001, pp 447–484.
15. Baldessarini, R. J., Tarazi, F. I. Drugs and the treatment of psychiatric disorders: psychosis and mania. In *The Pharmacological Basis of Therapeutics*, 10th ed.; Hardman, J. G., Limbird, L. E., Gilman, A.G., Eds., McGraw-Hill: New York, 2001, pp 485–520.
16. Comings, D. E.; Blum, K. *Prog. Brain Res.* **2000**, *126*, 325–341.
17. Dziuron, P.; Schunack, W. *Eur. J. Med. Chem.* **1975**, *10*, 129–133.
18. Carman-Krzan, M.; Krzan, M.; Schunack, W. *Naunyn-Schmiedeberg's Arch. Pharmacol.* **1997**, *355*, 431–437.
19. Leschke, C.; Elz, S.; Garbarg, M.; Schunack, W. *J. Med. Chem.* **1995**, *38*, 1287–1294.
20. ter Laak, A. M.; Timmerman, H.; Leurs, R.; Nederkoorn, P. H.; Smit, M. J.; Donne-Op, K. G. *J. Comput. Aided Mol. Des.* **1995**, *9*, 319–330.
21. Kramer, K.; Elz, S.; Pertz, H. H.; Schunack, W. N. *Bioorg. Med. Chem. Lett.* **1998**, *8*, 2583–2588.
22. Elz, S.; Kramer, K.; Pertz, H. H.; Detert, H.; ter-Laak, A. M.; Kuhne, R.; Schunack, W. *J. Med. Chem.* **2000**, *43*, 1071–1084.
23. Elz, S.; Kramer, K.; Leschke, C.; Schunack, W. *Eur. J. Med. Chem.* **2000**, *35*, 41–52.
24. Carman-Krzan, M.; Bavec, A.; Zorko, M.; Schunack, W. *Naunyn Schmiedeberg's Arch. Pharmacol.* **2003**, *367*, 538–546.
25. Wyrick, S. D.; Booth, R. G.; Myers, A. M.; Owens, C. E.; Kula, N. S.; Baldessarini, R. J.; Mailman, R. B. *J. Med. Chem.* **1993**, *36*, 2542–2551.
26. ter Laak, A. M.; Timmerman, H.; Leurs, R.; Nederkoorn, P. H.; Smit, M. J.; Donne-Op den Kelder, G. M. *J. Comput. Aided Mol. Des.* **1995**, *9*, 319–330.
27. Bucholtz, E. C.; Brown, R. L.; Tropsha, A.; Booth, R. G.; Wyrick, S. D. *J. Med. Chem.* **1999**, *42*, 3041–3054.
28. Miyaura, N.; Suzuki, A. *Chem. Rev.* **1995**, *95*, 2457–2483.
29. Nesloney, C. L.; Kelly, J. W. *J. Org. Chem.* **1996**, *61*, 3127–3137.
30. Miller, B.; Shi, X.; Grosu, G.; Zhou, R. *J. Med. Chem.* **1993**, *58*, 2320–2323.
31. Cereghetti, M.; Marbet, R.; Schleich, K. *Helv. Chim. Acta* **1982**, *65*, 1318–1330.
32. Burckhalter, J. H.; Campbell, J. R. *J. Org. Chem.* **1961**, *26*, 4232–4234.
33. Borch, R. F.; Bernstein, M. D.; Durst, H. D. *J. Am. Chem. Soc.* **1971**, *93*, 2897–2901.
34. Molander, G. A.; Biolatto, B. *J. Org. Chem.* **2003**, *68*, 4302–4314.
35. Booth, R. G.; Moniri, N. H.; Bakker, R. A.; Choksi, N. Y.; Nix, W. B.; Timmerman, H.; Leurs, R. *J. Pharmacol. Exp. Ther.* **2002**, *302*, 328–336.
36. De Lean, A.; Stadel, J. M.; Lefkowitz, R. J. *J. Biol. Chem.* **1980**, *255*, 7108–7117.
37. (a) Ghoneim, O. M.; Booth, R. G. *Soc. Neurosci. Abstr.* **2003**, *28*, 891.6; (b) Ghoneim, O. M.; Booth, R. G. *Am. Chem. Soc. Abstr. (SERMACS)* **2004**, *56*, 12820.
38. Legere, J. A.; Moniri, N. H.; Booth, R. G. *Am. Chem. Soc. Abstr.* **2003**, *225*, 239.
39. Kroeze, W. K.; Kristiansen, K.; Roth, B. L. *Curr. Top. Med. Chem.* **2002**, *2*, 507–528.
40. Psychoactive Drug Screening Program (PDSP); B. L. Roth, Director. NIMH Contract NO2MH80002, Case Western Reserve University, Cleveland, OH, **2005**.
41. Porter, R. H.; Benwell, K. R.; Lamb, H.; Malcolm, C. S.; Allen, N. H.; Revell, D. F.; Adams, D. R.; Sheardown, M. J. *Br. J. Pharmacol.* **1999**, *128*, 13–20.
42. Wyrick, S. D.; Booth, R. G.; Myers, A. M.; Owens, C. E.; Bucholtz, E. C.; Hooper, P. C.; Kula, N. S.; Baldessarini, R. J.; Mailman, R. B. *J. Med. Chem.* **1995**, *38*, 3857–3864.
43. Martin, Y. C.; Bures, M. G.; Dahaner, E. A.; Delasser, J.; Lico, I.; Pavlik, P. A. *J. Comput. Aided Mol. Des.* **1993**, *7*, 83–102.
44. Golbraikh, A.; Tropsha, A. *J. Mol. Graph. Model* **2002**, *20*, 269–276.
45. Savarese, T. M.; Fraser, C. M. *Biochem. J.* **1992**, *283*, 1–19.
46. Ohta, K.; Hayashi, H.; Mizuguchi, H.; Kagamiyama, H.; Fujimoto, K.; Fukui, H. *Biochem. Biophys. Res. Commun.* **1994**, *203*, 1096–1101.
47. Wang, C. D.; Gallaher, T. K.; Shih, J. C. *Mol. Pharmacol.* **1993**, *43*, 931–940.
48. Kristiansen, K.; Dahl, S. G.; Edvardsen, O. *Proteins* **1996**, *26*, 81–94.
49. Kristiansen, K. *Pharmacol. Ther.* **2004**, *103*, 1–80.
50. Zingel, V.; Elz, S.; Schunack, W. *Eur. J. Med. Chem.* **1990**, *25*, 673–680.
51. Bucholtz, E. C.; Wyrick, S. D.; Owens, C. E.; Booth, R. G. *Med. Chem. Res.* **1998**, *8*, 322–332.
52. Roth, B. A.; Shapiro, D. A. *Expert Opin. Ther. Targets* **2001**, *5*, 685–695.
53. Bos, M.; Jenck, F.; Martin, J. R.; Moreau, J.-L.; Sleight, A. J.; Wichmann, J.; Widmer, U. *J. Med. Chem.* **1997**, *40*, 2762–2769.
54. Traiffort, E.; Leurs, R.; Arrang, J. M.; Tardivel-Lacombe, J.; Diaz, J.; Schwartz, J. C.; Ruat, M. *J. Neurochem.* **1994**, *62*, 507–518.
55. Cheng, Y. C.; Prussof, W. H. *Biochem. Pharmacol.* **1973**, *22*, 3099–3108.
56. Cramer, R. D., III; Patterson, D. E.; Bunce, J. D. *J. Am. Chem. Soc.* **1988**, *11*, 5959–5967.
57. Wolfe, J. P.; Rennels, R. A.; Buchwald, S. L. *Tetrahedron* **1996**, *52*, 7525–7546.
58. Adamczyk, M.; Watt, D. S. *J. Org. Chem.* **1984**, *49*, 4226–4237.
59. Itoh, K.; Miyake, A.; Tada, N.; Hirata, M.; Oka, Y. *Chem. Pharm. Bull.* **1984**, *32*, 130–151.
60. Ghoneim, O. M.; Covington, D. W.; Moniri, N. H.; Booth, R. G. *Soc. Neurosci. Abstr.* **2002**, *28*, 249.5.
61. Wislicenus, W.; Grutzner, R. *Chem. Ber.* **1909**, *42*, 1930–1940.
62. Boots Pure Drugs, Patent FRM 5737, 1964; *Chem. Abstr.* **1969**, *70*, 114837d.
63. Pendergast, W.; Johnson, J. V.; Dickerson, S. H.; Dev, I. K.; Duch, D. S.; Ferone, R.; Hall, W. R.; Humphreys, J.; Kelly, J. M.; Wilson, D. C. *J. Med. Chem.* **1993**, *36*, 2279–2291.